CHALMERS

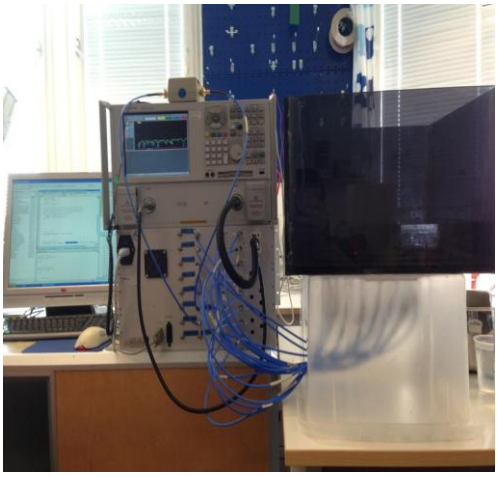

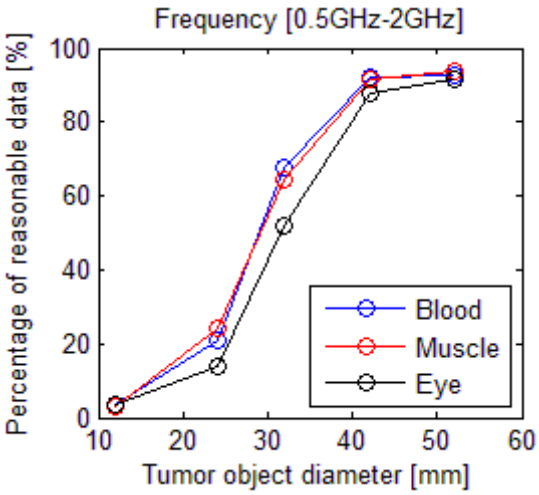

Microwave-based temperature monitoring: Sensitivity to temperature changes

Master of Science Thesis in the Master Program of Biomedical Engineering

YOUSEF GOUDA

Department of Signals & Systems
Biomedical Engineering
Chalmers University of Technology
Gothenburg, Sweden 2013
Report number: EX004/2014

Abstract

Microwave based temperature imaging is a non-invasive temperature measurement method which is necessary during hyperthermia treatment for monitoring purposes and dose evaluation. This thermometer imaging system is still a problem that must be solved before hyperthermia can be launched as an effective tool for cancer treatment. Some clinically available applications today such as MRI or invasive catheters have many problems, while the advantage of microwave monitoring system is that the same antenna array can be simultaneously used in thermal imaging and hyperthermia treatment. However, the aim of this thesis is to determine the feasibility of using microwave thermal imaging in order to estimate its sensitivity to temperature changes. This thesis is based on both simulated and experimental data which were performed to estimate the temperature changes of single heated tumor object inside the phantom. Simulations were implemented in two configurations, first one without defining the containers which include the phantom and the internal tumor object. Second configuration was performed by defining the two containers which have been implemented to verify the experimental results. Later, experimental measurements were performed by using containers due to the liquid phantoms to find out systems feasibility to measure temperature changes practically. The internal tumor object was tested with different diameters, temperatures and positions. Dielectric probe was used to determine thermal dependence of dielectric properties for eye, blood and muscle phantoms in the frequency range 100MHz to 2GHz. Different simulations were performed using finite difference time domain FDTD method based on the conductivity σ and permittivity ϵ of specific phantoms. Later, twenty monopole antennas arranged in a 200mm diameter circle were used to generate microwaves in the frequency range 0.4 to 2GHz. This system could reveal tumor's temperature changes under certain conditions while it still requires more improvements under some other conditions. The results showed that the system has high potential to estimate temperature changes without using the containers. Moreover, tumor object diameter is considered as primarily factor that affects the results, where at 32mm diameter the results began to demonstrate an appropriate transmission coefficient difference between two various temperatures up to 7dB. Simulation and measurement results displayed high decline in the temperature changes by using the containers. The results showed however a good transmission coefficients agreement between simulation and experimental results.

Acknowledgment

I would like to express my deepest appreciation to my supervisor Dr. Hana Dobsicek Trefna for her guidance, support and effort during my thesis work. In addition, a special thank goes to my examiner Dr. Andreas Fhager for his remarks and really effective and useful comments. I am very honored and grateful for their time, kindness and for providing me the opportunity to work in biomedical electromagnetic group at Chalmers University of Technology. Thesis topic was so interesting for me since it is related to such research in cancer field and its treatment devices. Thus gave me the motivation to accept this thesis as well as the diversity of research method between numerical simulations and laboratory work. Besides, I am also thankful to my friend Shaochuan Li for our cooperation in some similar parts between my and his thesis.

Yousef Gouda, Göteborg, 30 August 2013

Contents

1

Introduction

Cancer disease is increased from one year to other in many different countries around the world. The statistics shows that everybody has a risk more than 30% in their live to have a cancer [1]. Incidence of cancer has increased in Sweden by an average of 2.0% for men and 1.4% for women each year in the last two decades. In 2010, 44964 people in Sweden were diagnosed with cancer in their first time. In the same year, 422 cancer diagnoses cases in children and adults under 20 years old [1]. The distribution is relatively between sexes, 52% of cancers diagnoses in men and 48% in women. Based on these statistics, Different cancer treatment methods have to evolve in order to protect hundreds of patients. Thus, to reduce the spread of cancer disease as well as to achieve a cure in a comfortable and simple way [1].

Hyperthermia is one method which is used for cancer treatment. The aim of this method is to kill the tumor by elevating the temperature to 41-45℃ [2]. This thesis will however not focus on the hyperthermia itself, but it will focus on microwave based thermal monitoring which is necessary during hyperthermia treatment. This method has potential to monitor three dimensional 3D temperature distributions in the treated area. Increasing the temperature above 42℃ in the healthy tissue during hyperthermia treatment may burn the tissue [2]. Hence it's clearly shown the importance of the thermal distribution monitoring during the treatment in order to avoid this effect. In this thesis the focusing will handled in determining the feasibility of using microwave thermal imaging in order to estimate its sensitivity to temperature changes in hyperthermia range.

The report is organized in five main chapters. Background describes in detail the definition of hyperthermia technique and the importance of thermal monitoring system. Methods and materials chapter covers the approaches that have been followed to reach the desired results. This chapter also presents different equipments which were used in the research. Later, several forms of temperature changes results which were simulated and measured are shown in chapter four. The results are discussed and concluded in chapter five and six respectively. Finally, further work Suggestions are discussed separately as well in chapter seven.

2

Background

This chapter is a general overview which describes different cancer treatment systems that are clinically available nowadays. This chapter will also cover the importance of using thermal distribution monitoring, different invasive and non invasive temperature distribution methods, previous studies of microwave based thermometry and finally the aim of this thesis.

2.1 General Overview of cancer treatment:

Cancer is generally treated using three main modalities which are surgery, chemotherapy or radiation therapy. Surgery is often the most effective method which depends on the lumpectomy. The chemotherapy anti cancer drugs are delivered into the body in order to control cancer cells spreading. Moreover, heating the tumor by using microwaves can exploit as well in order to make the tumor tissue more sensitive to the microwaves effect. Hyperthermia method is based on killing tumor cells by elevating its temperature to 41-45℃. Increase the oxygenation of the tumor is one important factor which hyperthermia depends on to kill the tumor [4]. However, using cancer treatment methods in inaccurate way may lead to damage the human body. Cytotoxic effect can happen either on cancer cells or healthy cells If the therapy temperature exceed above the required degree. Also, temperature's increasing can corrupt the protein, prevent cellular repairing process and prevent the formation of blood vessels (angiogenesis). Furthermore, hyperthermia may cause death of cells in any type [2, 3, 6]. Optimal hyperthermia treatment requires heating of the cancer cells only and to protect the surrounding healthy tissue from this heating as much as possible.

Local hyperthermia, Regional or part-body hyperthermia and whole body hyperthermia are the main three types which will be explained in order to get the general overview [2]. The most used type is local hyperthermia which using operating frequencies between 400 MHz and 2.45 GHz. Local hyperthermia operating frequency provides treatment for tumor which is placed at a depth of less than 3cm [2, 4].

Deep hyperthermia is using annular phased array for tumor treatment which is located deeply in the body as shown in figure 1. Deep HT is typically applied by using antenna arrays placed around the injured body. For example, twenty antennas in circular shape are placed around the body section which contains the tumor. Furthermore, the affected body will be placed inside the antenna arrays and immersed in a water bolus. Several areas that regional HT can treat are for instance arm, leg while deep sections can be for example prostate, cervix or bladder. This type of HT is using different operating frequencies which depends on the cancer location. For instance, frequency between 70 and 200 MHz are suitable for cancer in the pelvic area while higher frequencies (e.g. 434 MHz) is recommended for head and neck therapy [2, 5].

Last technique is whole body hyperthermia which is used for metastatic or spread cancer. Similarly to previous techniques, whole body temperature must be increased to approximately 41℃ for about one hour. High temperature in whole body helps the tumor to be more suitable to annihilate by chemotherapy. The treatment in this modality is performed by using different heating methods such as electromagnetic induction or thermal conduction. The disadvantage of this method is its side effects which include vomiting and nausea [2, 5].

Figure 1: Annular Phased Array

2.2 Methods for monitoring temperature distribution:

Hyperthermia monitoring technique is necessary in order to determine thermal effect and thermal dose inside the body either on the cancer or healthy tissues. Furthermore, 3D temperature distribution monitoring ensure a hyperthermia treatment validation for individual patient. This technique provides a relation between treatment efficiency and thermal parameters received by the patient, figure 2. Moreover, this method guarantees high quality assurance as well as high treatment efficiency. In general, knowing the temperature distribution in the treated object during the treatment will help the improvement in different areas, such as to know if the temperature of the cancer tissue is elevated to the required temperature degree or not and to guarantee that the cancer cells don't exceeded above the required temperature. It will also avoid temperature increasing in the healthy tissue which surrounds the cancer (forming hot spots). Furthermore, it will guide the treatment evaluation by giving the possibility to measure thermal distribution changing inside the treatment object [2, 6, 7, 8].

Non-invasive and invasive methods are two main procedures which are used in order to measure the temperature distribution during the treatment. Moreover, it's reasonable to use invasive method in local hyperthermia due to its higher accuracy while non-invasive method is more recommended for deep hyperthermia modality [2].

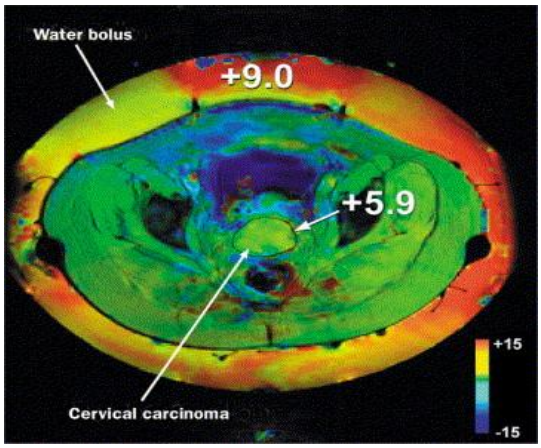

Figure 2: Temperature distribution example of a non-invasive measurement [12]

2.2.1 Invasive temperature distribution methods:

The objective of invasive methods is to measure the temperature distribution during the treatment by using a group of 10 fiber optic probes with diameter ranging from 0.5 to 1 mm for each probe. Some points have been mentioned by many authors which should be considered during the invasive thermometer improvements. These points can be summarized in the probe diameter which must be lower than 1.1 mm, thermometer change with time should be less than $0.1℃/\text{hour}$, thermometer accuracy should not be more than $\pm 0.2℃$, thermometer probe should not be excited by other heat source as well as insensitive to moisture and finally the standard deviation should be equal to or less than $\pm 0.01℃$ [9]. If tumor is located in someplace near the superficial then the probes can be placed in the surface. Catheters is recommended procedure that should be used for invasive temperature monitoring which can be inserted inside the patient using CT guidance. It's important to use CT for catheter placing especially in deep locations and for critical structures. Usually, patients and physicians prefer to use the catheters because it can be placed only once for all different treatment periods. Moreover, it saves the time for the physicians due to the same reason as well as it provides lower cost.

Figure 3 shows three main types of invasive catheters which are stylet insertion type catheter, standard needle insertion catheter and splittable needle insertion catheter. However, several devices can be used instead of the fiber optics which can similar purpose such as thermistor. The principle idea of thermistor is based on calculating the resistance as a function of the temperature. This computation can be performed by transfer a small current value from one side, while other side is using for calculate the voltage decreasing. Other low cost device which can be used are thermo-couples [2, 9].

Invasive thermometry method is no sufficient and still need improving because it appears only few temperature points. Therefore, the new system is really recommended and important which can shows the temperature data in more detail as well as the three dimensional distribution.

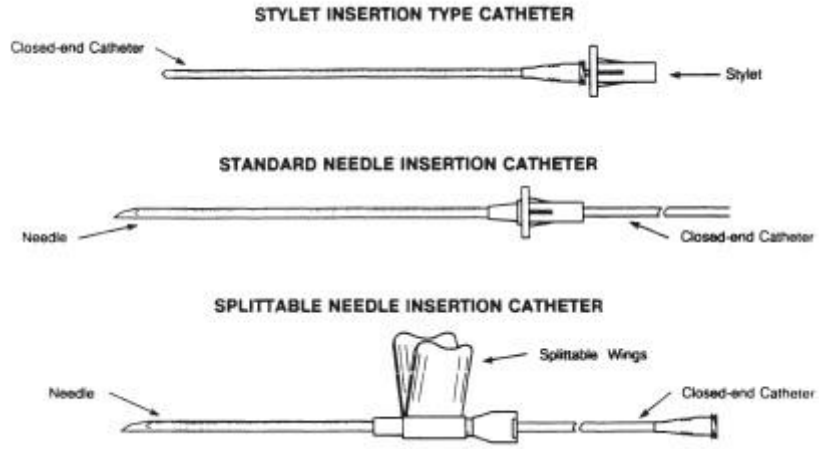

Figure 3: The three main catheters which are using in invasive temperature monitoring [10]

2.2.2 Non invasive temperature distribution methods:

Magnetic Resonance Imaging (MRI) [15], ultrasound [2] and microwave tomography [16] are different non-invasive devices used in thermometry. MRI is the most advanced method with drawback of high price. Therefore, the other methods are preferred due to its lower price. Several developments are currently ongoing in order to make some improvements [2].

MRI depends on different temperature sensitivity parameters which are currently exploited for thermometer monitoring. These are T1 and T2 relaxation time of water protons, proton resonance frequency shift (PRFS), diffusion coefficient and magnetization transfer. The relation between T1 and temperature changing is almost linear while the relation between T2 and temperature changing is nonlinear. T1 and T2 relaxation are frequency dependent. Which implies that temperature difference cause changing in T1 and T2 relaxation time. This relaxation difference is the objective which build up images [15]. Furthermore, T1 is preferred for low field systems due to its higher contrast. However, this method has low accuracy and sensitivity due to its long relaxation time, therefore it's not recommended for small T1 changes. Using T1 in temperature monitoring can be driven in faster way by using dynamic contrast enhanced MRI (DCE-MRI). T1 has also potential to monitor laser ablation which is a method that depends on using temperature above 50℃ to burn small tumors [15].

PRFS estimate the temperature change based on the proton frequency of tissues water. The most recommended is to use PRFS method for magnetic fields ≥1 Tesla. Changing water's temperature cause change in the frequency peak. This peak differences build up the image. This method has significant high accuracy to temperature change except for fatty tissue. This happen due to that fat molecules alter the PRFS and this occur temperature error. Diffusion coefficient is the method which is not available for clinical application until now due to some technical limitations. However, this method depends on temperature dependence of the diffusion coefficient [11]. Magnetization transfer MT may also be perform in temperature monitoring based on different exchange processes. However, this method doesn't has high sensitivity [15]. MRI monitoring technique can be more enhanced by using injection contrast agent. Moreover, the relation between the contrast agent and the temperature can be either linear or non linear. Linear agent such as Pr-MOE-DO3A which provide a chemical shift of spectral line. Non linear agent transmits using liposomal carriers in which the agents emitted from the carriers at certain temperature [2, 10, 11, 15].

The working principle of ultrasound device in the thermometer monitoring area is based on the relation between the temperature factors of sound speed and thermal extension factors [2]. However, MRI and ultrasound methods still suffers from some limitations such as organ motion artifacts like heart and breath moving [2, 10, 11].

2.2.3 Microwave based thermometry:

Microwave tomography imaging is a non invasive temperature monitoring system which is based on using the antennas array to monitor the temperature distribution in the treated area. However, this method require more development and researches until it can be launched as a thermometry effective tool. Several studies have been performed in this field at different periods of time. Starting with an old paper in 1983, Bolomey et al. [17] showed the feasibility of using microwave imaging to remote thermal sensing. Their imaging experiment was based on the permittivity differences of tissues. Later in 1993, M. Miyakawa. [16] explored the possibility of using the microwave tomography in order to measure the temperature changing in body phantoms. The experiment was done by transmitting radiation on the body and the scattered waves were received by antennas in the opposite side. Chirp pulse signal was using in the frequency range between 1 and 2GHz. This method was succeed to image parts with complicated dielectric structures but on the other hand it was not reasonable for high contrast objects. Other previous study in 2012 by Helbig et al. [18] showed an experiment on heterogeneous breast phantoms based on M-sequence radar technology and small active antennas. Their results showed the possibility of this system to be either used to image more than one tumor inside the body.

Meaneys group made a number of experiments efforts in microwave thermometry. In 2003, [20] they showed, by using their log-magnitude and phase reconstruction algorithm, the temperature distribution based on phantoms dielectric properties. The experiments were performed by using a single heated saline tube of 5.1cm diameter. Two monopole antenna arrays with different diameters (15 and 25cm) were utilized individually. The results demonstrated high temperature tracking accuracy up to 0.2℃ instead of 1.6℃ which was observed in the previous experiments. Later in the same year, [21] they made a microwave tomographic imaging in the frequency range 300-1000MHz to show heat saline object which was inserted surgically on a pig. The images which were reconstructed in the same frequency range demonstrated different results which changes based on the temperature values. The tube which was using for saline injection is clearly shown. Recently in 2008, [22] they used high intensity focused ultrasound system to arbitrarily heat different phantom zones. Three different heating patterns have been scanned which are circle with 6.5cm diameter, 240° arc of a circle with 4.8cm diameter and scanning a spirals of a 1.6cm diameter. These three heating areas have been successfully monitored using microwave tomographic imaging. The system sufficiently demonstrated the temperature differences with sensitivity higher than 0.5℃.

Recently in 2010, Hana D. Trefna et al. [19] made a microwave tomographic imaging experiment to show its temperature monitoring feasibility. Their study was based on FDTD simulation of the electromagnetic problem as well as the laboratory work. Experimental and simulation results shows the possibility of temperature estimation. The paper shows an agreement between these results and image reconstructions based on four different temperatures: 25, 30, 35 and 40℃. The second important conclusion in this paper is the ability of using appropriate phantoms instead of real tissues. From this result, we got the possibility of using several tissues equivalent phantoms in this thesis.

2.3 The main purpose of this thesis:

The aim of this thesis is to determine the feasibility of using microwave thermal imaging in order to estimate its sensitivity to temperature changes. The principle of measuring the spatial temperature distribution is based on determining the permittivity σ and conductivity ε values in tissue equivalent phantoms. Later, the 3D simulation based on the dielectric properties results will be performed. Finally, the same tests will be performed experimentally to proof the agreement between simulated and measured results.

3

Materials and Methods

The work in this thesis is divided into three main parts. First, dielectric properties measurements were performed on some tissue-equivalent phantoms. The aim of coming two parts were to estimate the sensitivity of microwave thermal imaging to temperature changes. Simulation part was performed by using FDTD modelling and third part was laboratory experiments.

3.1 Thermal dependence of dielectric properties:

Tissue equivalent phantoms of head and neck have been used in the lab instead of using tissues. The three different phantoms which were tested represents blood, eye and muscle. Blood phantom consists of 30% sugar, 1.2% salt and water. Eye phantom consists of 50% glycerol, 49% water and 1% salt. Muscle phantom consists of 40% sugar, 0.6% salt and water.

The experiment was performed as follow. The phantom was heated up to approximately 50℃ by using standard electric heater. The dielectric probe (85070E, Agilent) was calibrated and kept in fixed position, while the heated phantom cup must be stable in order to avoid any air bubble formation on the probe. The probe was set and kept fixed in the first quarter of the heated phantom cup as shown in figure 4. The temperature was calculated during the measurement by using luxtron thermometer (755), which has been used in order to measure accurate phantom temperature [14]. Three thermometer channels were attached upper first quarter of the phantom as indicated in figure 5. VNA system consists of three main units which are source unit, receiver unit and a display unit. The probe emits a signal of a specific frequency which then will detect the dielectric properties of the phantom and will be shown on the display unit.

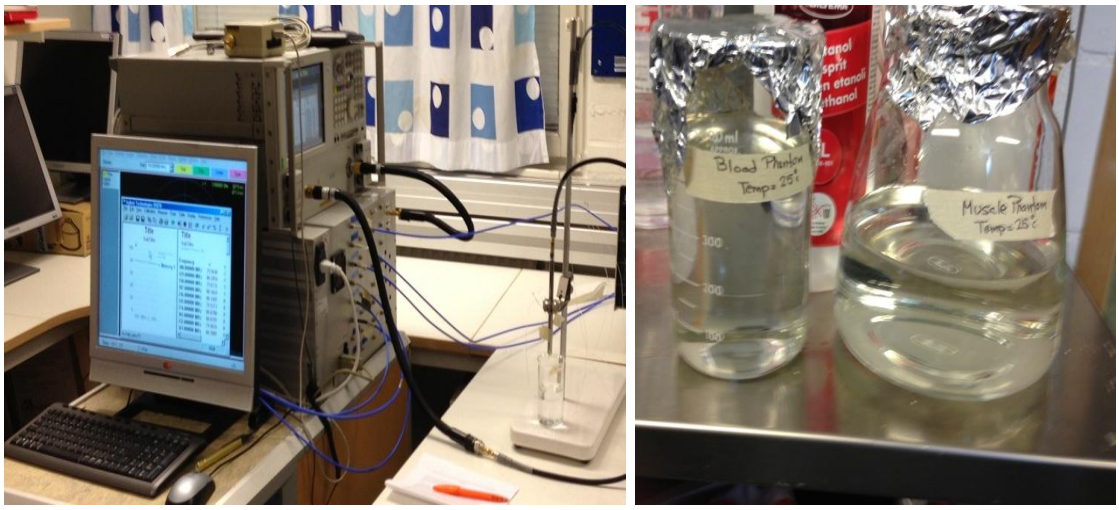

(a) (b)

Figure 4: (a) Vector Network Analyzer Unit during measuring the dielectric properties of a specific phantom. Dielectric probe (85093E, Agilent) is immersed inside the phantom in the glass cup which can be shown in the right side of the figure. (b) Prepared blood and muscle phantoms with 25℃.

VNA was measuring real and imaginary part of the permittivity every 1℃ decrease in the frequency range 100MHz to 2GHz. Dielectric properties of the phantoms, i.e. conductivity σ and permittivity ϵ, were calculated through equations 3.1 and 3.1 using Matlab:

$$\epsilon^* = \epsilon_o(\epsilon' - j\epsilon'') = \epsilon_o\left(\epsilon_r - j\frac{\sigma}{\omega\epsilon_\circ}\right) \qquad 3.1$$

$$\sigma = \epsilon'' * \epsilon_o * (2\pi f) \qquad 3.2$$

Where ϵ'' and ϵ' are imaginary and real permittivity parts respectively, while ϵ_o is the permittivity of free space which is equal to $8.854 * 10^{-12}$ farads per meter. Finally, dielectric properties values were plotted versus temperature range 25 to 50℃ for different frequencies.

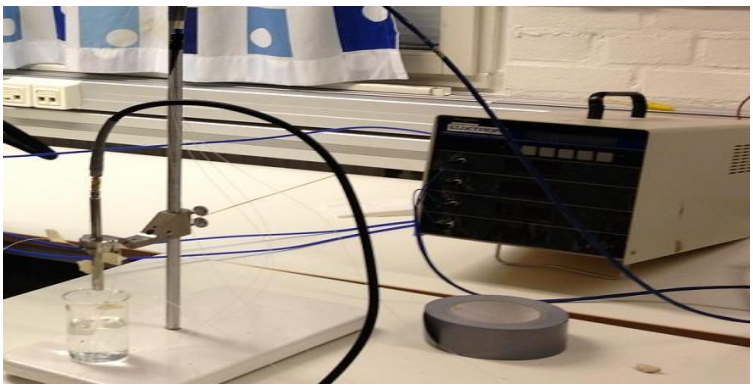

Figure 5: Luxtron 755 thermometer during measuring temperature changes of specific phantom.

3.2 Sensitivity to thermal changing of dielectric properties:

The aim of the simulation is to determine the sensitivity of a microwave antennas system to the dielectric properties changes measured in part 3.1. Finite difference time domain FDTD algorithm was performed to numerically model the waves propagation which transmit from the monopole antennas. For each measurement or simulation, a multistatic data matrix S is obtained. S matrix describes the input/output relation between two antennas. For instance, S1-1 antenna represents the return loss of antenna number 1. Figure 6 illustrates an example of S1-10, where it measures power transferred from antenna 1 to antenna 10. Figure 9a shows plot example of data matrix S of four different antennas. Each S matrix, for instance S1-10, present real and imaginary part of the permittivity in the frequency range 0.4 to 2GHz

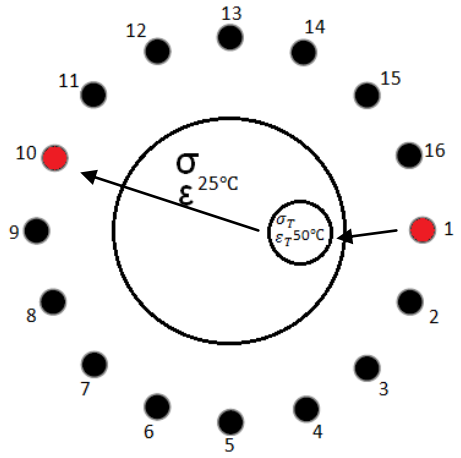

Figure 6: Illustration of transmitter and receiver of multistatic matrix S1-10.

3.2.1 Implementation of FDTD modeling using C^{3}SE:

The permittivity and conductivity values were extracted from the data given by the dielectric properties measurements. Permittivity and conductivity values were taken at 1GHz, where it represents an average frequency (table 1). In the simulation system twenty monopole antennas mounted above a ground plane. 3D-FDTD model type was performed by using Gaussian pulse with 1GHz center frequency and 1GHz bandwidth. We used 2mm spatial resolution and the resistive voltage source with 50 Ω impedance. Perfect electric conductor PEC was used to model a ground plate of the antenna array. All simulations were performed by using Chalmers cluster C^{3}SE. Using this computer cluster was useful due to its high speed and the ability to run many simulations in sequential. The specific dielectric properties (i.e. conductivity and permittivity) were changed by using different data files affiliated to the main FDTD code.

Eye phantom	50°C	Permittivity=59.13 Conductivity=1.8 S/m
	25°C	Permittivity=62.72 Conductivity=1.316 S/m
Blood phantom	50°C	Permittivity=61.79 Conductivity=2.4 S/m
	25°C	Permittivity=65.41 Conductivity=1.716 S/m
Muscle phantom	50°C	Permittivity=65.01 Conductivity=0.9604 S/m
	25°C	Permittivity=65.57 Conductivity=0.4819 S/m

Table 1: Dielectric properties values at 1 GHz which were using for experiments and simulations.

3.2.2 Simulation setup:

Simulation work was performed in two main configurations. The first was implemented by make a 25°C large phantom with 100mm diameter which was placed in the center of the antenna array. Other phantom with 20mm diameter and specific tumor conductivity σ_T and permittivity ϵ_T assumed to be the tumor object. This tumor object was setting inside the large phantom. The different radiuses which were tested for the tumor object are 6, 12, 16, 21 and 26mm. Each of these radiuses have been tested with different temperatures starting with 25, 30, 35, 40, 45 and 50°C. Achieving the desired temperature was identifying by setting its specific σ_T and ϵ_T according to the description in section 3.1. The tumor spot was also tested in two different positions, first position was at the center of the array and second position set close to the wall. Figure 7 illustrates an example of two different simulation setups where the two tumor spots have different temperatures and locating close to the wall (i.e. antenna number 1). The whole assembly was simulated to be immersed in a water background with 100mm height in order to provide electromagnetic coupling between the surface and the antennas. Waters permittivity and conductivity were set as 78 and 0.1 respectively.

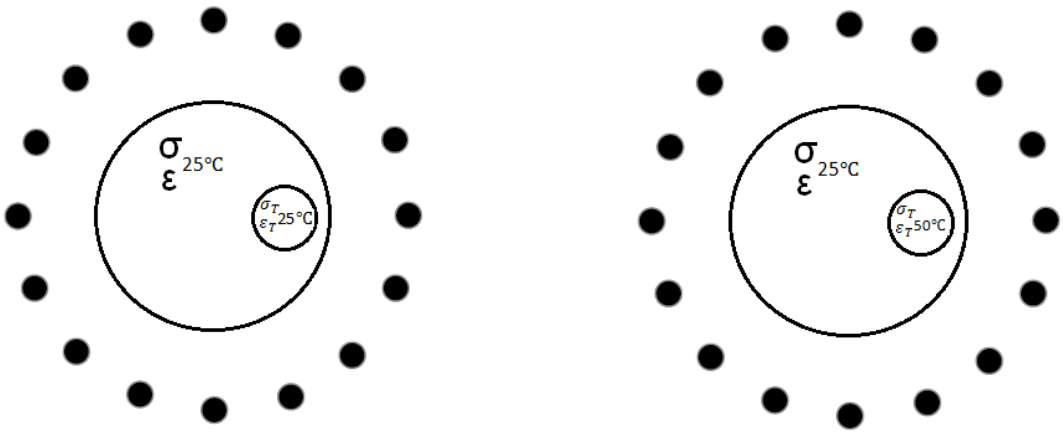

Figure 7: Illustration of two different simulation setups

Second simulation configuration was performed by assuming that the large phantom and the tumor phantom are placed inside a containers. The containers were simulated by defining its permittivity and conductivity of 2.2 and 0.07s/m respectively. The aim of this step is to simulate same experimental model in order to verify the measurement results. The large phantom diameter was 100mm while the two tested diameters of the tumor objects were 40 and 20mm. Each tumor object diameter has been tested under 25 and 50℃. Each of the tumor objects were tested first at the center of the large phantom and the second test was performed by setting it close to the wall as illustrated in figure 7.

3.3 Experimental setup:

The purpose of the experimental work is to estimate the sensitivity of microwave antennas to the temperature changes practically. Based on that, the measurement setup was kept similar to the second simulation configuration. Muscle and blood phantoms were prepared according to the description in section 3.1. Due to the liquid phantoms, it was necessary to have one container for the large phantom and other small container for the tumor object as shown in figure 8a. The antennas system consists of 20 monopole antennas, each of 19.5mm height, are arranged on a circle with diameter 200mm as shown in figure 8a. Every antenna is operated as a receiver and a transmitter and is coupling with the switching box through the blue wire. Vector network analyzer VNA (Agilent E8362) was utilized to determine the multistatic matrix. All antennas are fixed in a ground square plane with dimensions $250\mathrm{mm}^2$. This plane with the antennas are fixed inside the square black box tank with dimensions $370\mathrm{mm}^3$. The black box tank is made of Perspex sheet with 1cm thickness. Tap water of approximately 100mm height was filling in the tank to use it as background. The experiment was performed by made a 25℃ phantom which was placed inside a container with 100mm diameter. Later, same phantom type with 50℃ was placed inside 40 or 20mm container. Both containers were closed tightly and placed one time in the center and other time in the side.

3.3.1 Importance of existing antennas inside a water bolus:

The antennas assembly were immersed inside a water bolus for several reasons during the simulation and experimental work. The importance of using water bolus is to provide electromagnetic coupling between the phantom surface and the twenty antennas. The relative permittivity of the water is 78 while the permittivity of the phantoms varies between 50 – 70. This convergence in the permittivity values lead to provide the electromagnetic coupling. However, due to the significant difference of permittivity values between phantom surface and the air, i.e. Air Permittivity=1, most of the microwaves are reflected back when using air background instead of water. Furthermore, water bolus is standard part of hyperthermia treatment as it provides cooling of body surface.

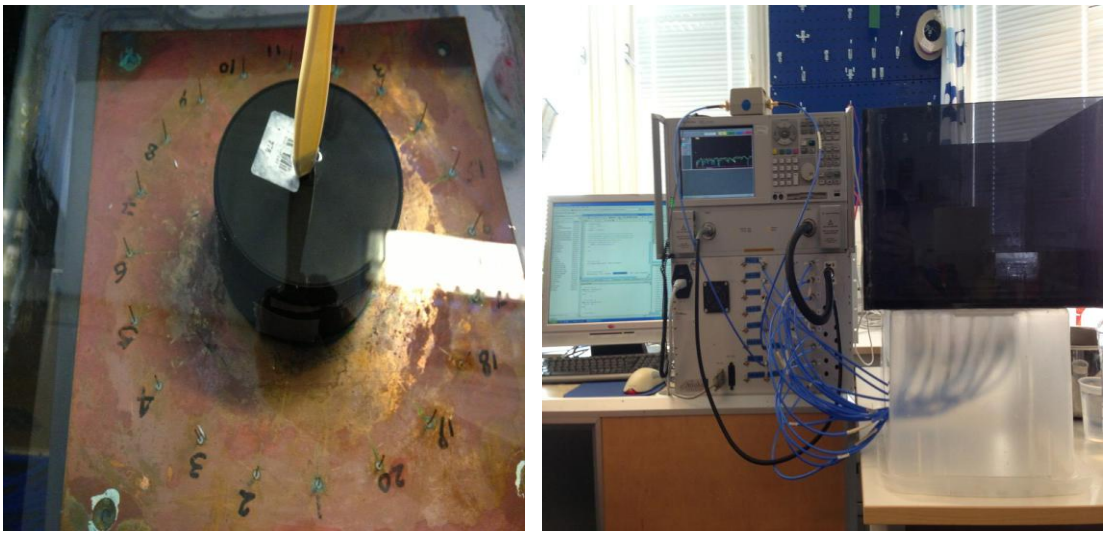

(a) (b)

Figure 8: (a) Large container filling with phantom placed inside the tank with water background. (b) photograph of the whole measurement system setup which shows the connection of the 20 antennas with the switching box.

3.4 Result Analysis:

The evaluator of temperature difference plots were performed by taking the difference between reference matrix S_{ref} (e.g. 25°C) and the higher temperature matrix S (e.g. 50°C) as shown in figure 9b. To create a relative change plot, the difference between two antennas should dividing by S_{ref}. The following are equations 3.3 and 3.4 which describes the above steps:

$$relative\ change\ (r) = \sum_{i=1}^{20} \sum_{j=1}^{20} \frac{\Delta}{S_{i,j\ (ref)}} = \frac{S_{i,j} - S_{i,j\ (ref)}}{S_{i,j\ (ref)}} \qquad (3.3)$$

In order to get the gain in logarithmic scale dB:

$$logarithmic\ relative\ change\ (r) = 20 * log10\ (r) \qquad (3.4)$$

Figure 9b, shows an example of relative change plots of four different antennas. It's clearly shown how this type of plots are recommended for numerically evaluation.

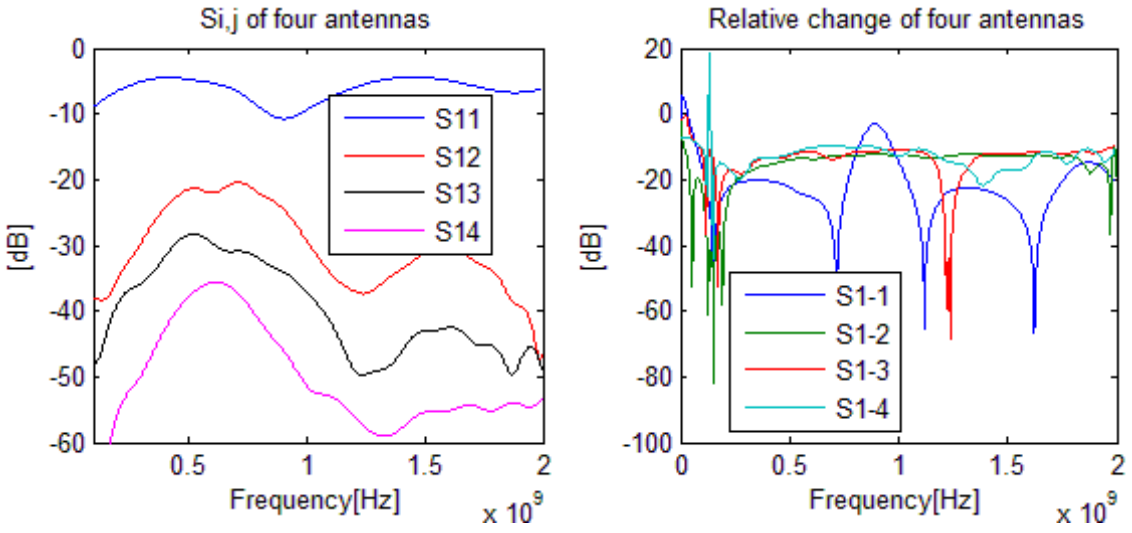

(a) (b)

Figure 9: (a) Transmission coefficients of four different data matrixes. (b) Relative change of four different data matrixes for muscle phantom.

Due to the huge amount of data, it was unreasonable to use relative change plots. A new method was performed which enables presenting a large number of antennas behaviour in one figure. This types of figures were implemented by plotting the transmission coefficients differences of two various S matrix temperatures $S(50℃) - S_{ref}(25℃)$ versus signal strength of reference matrix $S_{ref}(25℃)$ as shown in figure 10.

3.4.1 Reasonable data:

Reasonable data refers to the percentage of a certain region R of S matrix. This R region includes frequencies of S matrix which have temperature differences Δ larger than 1 dB and reference object strength S_{ref} stronger than -80dB as indicated in equation 3.5:

$$Reasonable\ data\ = \frac{\left|\{(\Delta,S_{ref})|(\Delta,S_{ref})\in R\wedge\Delta\geq 1\ \wedge S_{ref}\geq -80\}\right|}{|R|} * 100 \qquad (3.5)$$

Reasonable data boundaries have been identified since the noise increases too much at the signals which are weaker than -80dB. 1dB difference was identified as an appropriate interval between two various temperatures. The percentage of the reasonable data will be shown in each plot. In order to make the figures obvious and easier to read, the plots are dividing into three frequency ranges 0.5 to 1 GHz, 1 to 1.5 GHz and 1.5 to 2 GHz. Figure 10 shows a specific example of twenty different antennas from S1_1 to S1_20 with specific frequencies range 1 to 1.5 GHz. Each star in the plot represents temperature difference for specific frequency. Different S matrixes have been encoded with different colours as indicated in figure 13 (e.g. Blue colour represents S1_1).

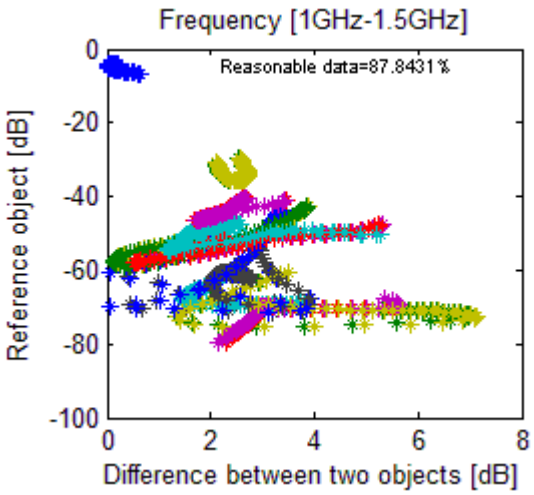

Figure 10: Twenty different multistatic matrix from S1-1 to S1-20 of eye phantom with small heating object locating close to antenna number 1.

4

Results

This chapter encompasses all the thesis results. Thermal dependence of eye, blood and muscle phantoms for specific frequencies are presented. Simulations and measurements transmission coefficient results as well as the effectiveness of implementing closer antenna array are also shown. Finally, antenna's sensitivity to different objects diameters as well as its ability to monitor small temperature tracking degrees are presented.

4.1 Thermal dependence of dielectric properties:

Figure 11 demonstrates the dependence of dielectric properties versus the temperature for blood, eye and muscle phantoms at four different frequencies. Measurements were performed based on the description in part 3.1. The aim of these plots were to identify phantom's dielectric properties at each one degree in the temperature range 21 to 51°C. These dielectric results will be utilized in the simulations and measurements test. Both simulation and measurement tests were performed based on the dielectric properties at 1.02GHz which represents an average frequency value. For instance, the permittivity value at 1.02GHz for blood phantom is 61.79 at 50°C, while it increased to 65.41 at 25°C. The permittivity of blood and eye phantoms show higher analogue in comparison with muscle phantom, where the values decreased in all frequency ranges. However, the permittivity of muscle phantom show less decreasing in all frequency ranges. This can be attributed to the salt concentration in each phantom, where the blood and eye phantoms include 1.2% salt whilst there is only 0.6% in the muscle phantom. The conductivity values of muscle and eye phantoms increased at low frequencies and show constant values at high frequencies. The conductivity of blood phantom increased in all frequency ranges.

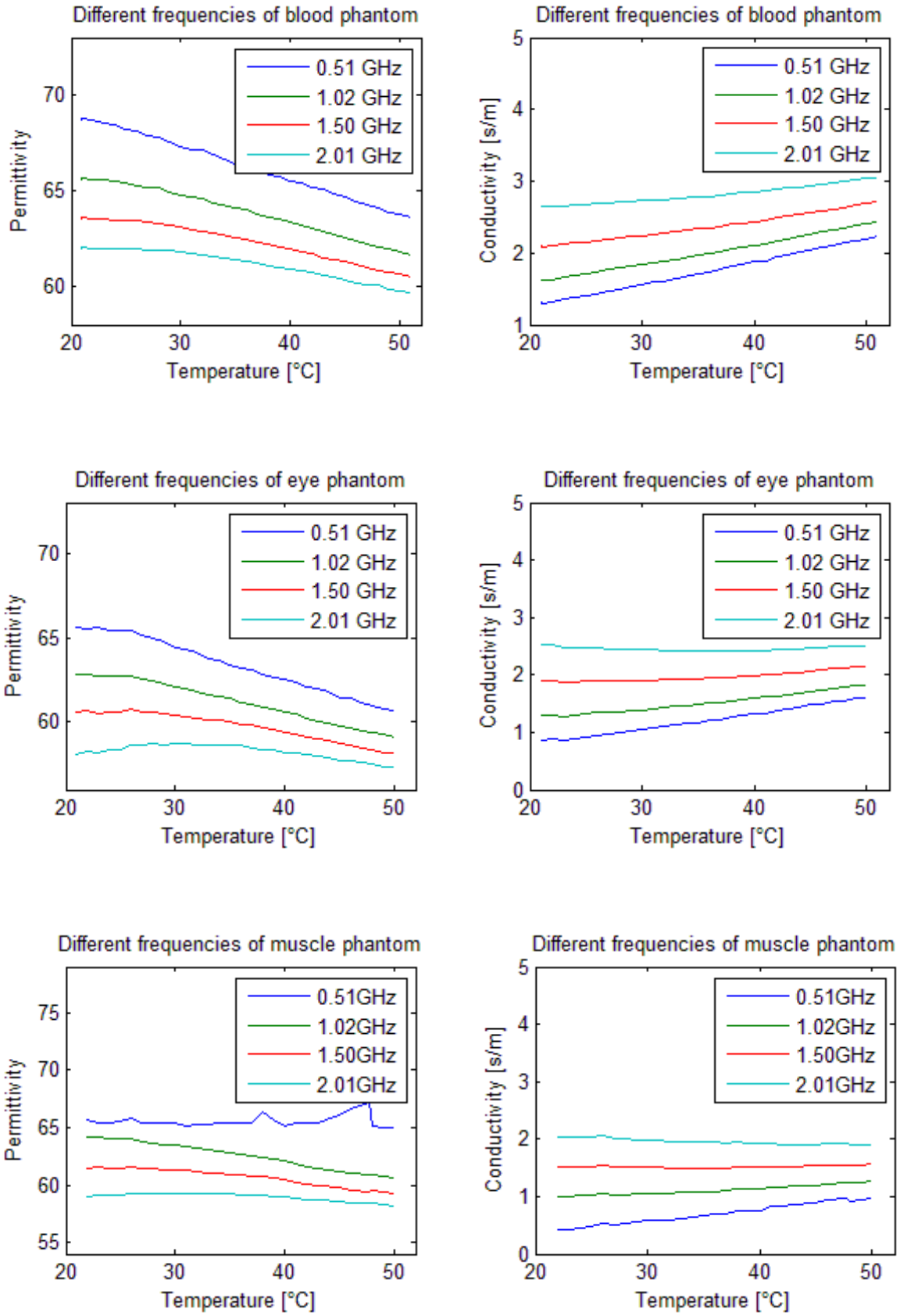

Figure 11: Dielectric properties of muscle, eye and blood phantoms versus temperature for different frequencies

4.2 Simulations transmission matrix results:

Figure 12 presents the transmission coefficients of certain S matrix versus frequency range 0 to 2 GHz. The results were simulated without defining the dielectric properties of the containers as described in section 3.2.2. Each plot shows the transmission coefficient differences of 50℃ and 25℃. Part a demonstrates the results of S11 and S12 when using tumor object of 40mm diameter. Part b demonstrates the results of S1-10 and S1-19 when using tumor object of 24mm diameter. Figure 12a shows high transmission coefficient differences [dB] between two temperatures up to 5dB. However, these differences become less significant by using 24mm tumor diameter to become approximately less than 1dB as shown in figure 12b.

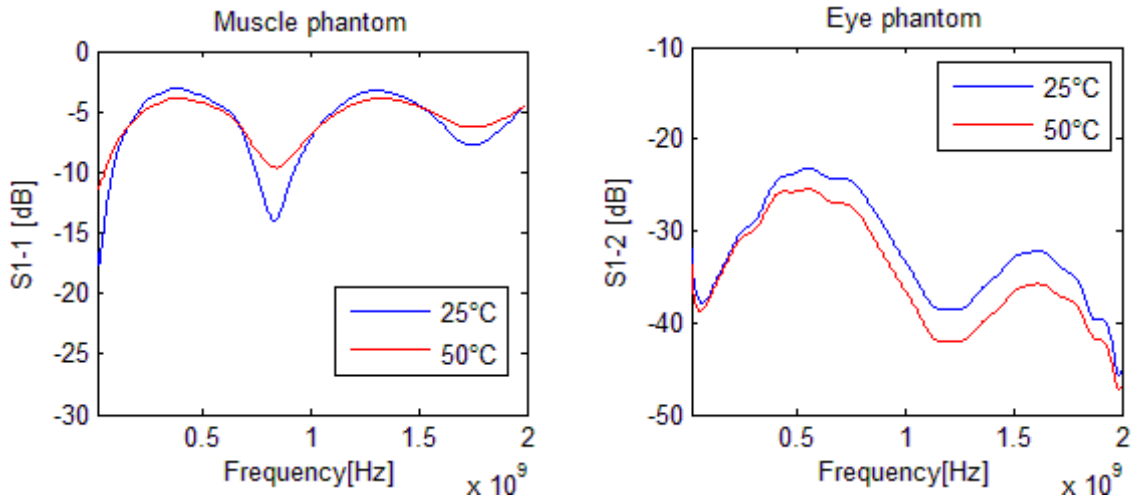

(a)

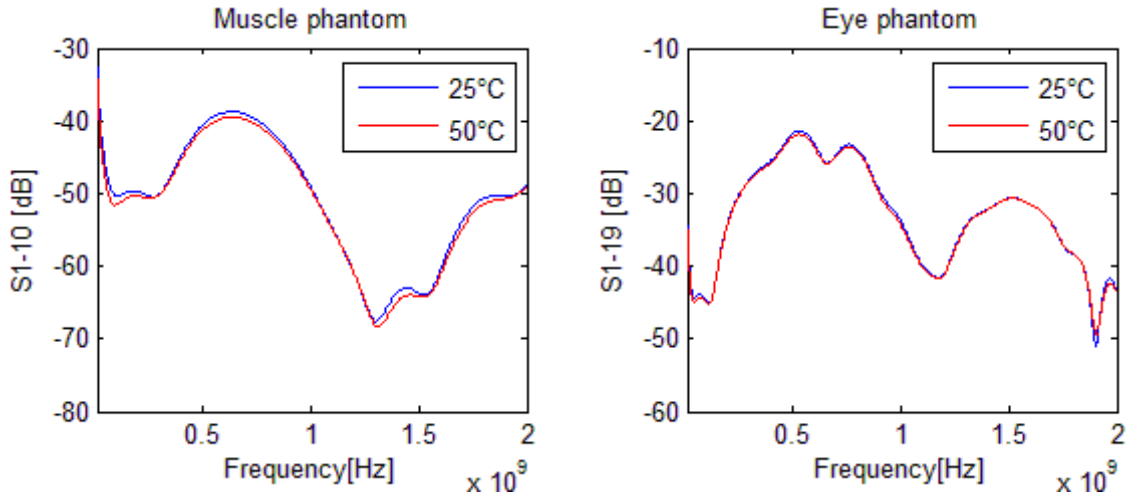

(b)

Figure 12: Transmission coefficients of various temperatures. (a) Using 40mm diameter of tumor object. (b) 24mm diameter.

4.3 Simulations temperature changes results

This part contains simulation results for blood, eye and muscle phantoms without defining the containers according to the description in section 3.2.2. The percentage of reasonable data, based on the description in section 3.4.1, is shown in each figure. Each plot represents the transmission coefficient differences of two various temperatures $S(50℃) - S_{ref}(25℃)$ versus signal strength of the reference matrix $S_{ref}(25℃)$. Different S matrixes have been encoded with different colours as indicated in figure 13.

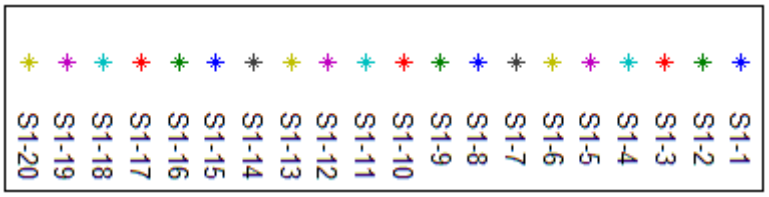

Figure 13: The main legend which represents all figures.

Figure 14 shows the transmission coefficients in three phantoms by using tumor object of 40mm diameter and is placed close to antenna number 1 as shown in figure 6. Plots a,b and c display the transmission coefficients of blood, eye and muscle phantoms respectively in the frequency range 500MHz to 1GHz. In addition, plot d displays muscle phantom in the frequency range 1.5 to 2GHz. The results show high reasonable data analogue in the range 94 to 97% as shown in each figure. The transmission coefficient demonstrates high differences between 50℃ and 25℃ in the range 1 to 10dB which is considered as a measurable difference. Furthermore, the signals are mostly placed in the range -20dB to -80dB which can also considered as a strong signal. All antennas which are close to antenna 1 show the stronger signals in all results due to close distance from the tumor. For instance, S11 which is shown in the blue stars demonstrates the strongest signal in the range -5dB due to the close reflection. Moreover, figure 14a shows S13 in the red stars which presents high transmisson coefficient differences up to 14dB. All results which were simulated by using 40mm tumor diameter show high percentage of reasonable data.

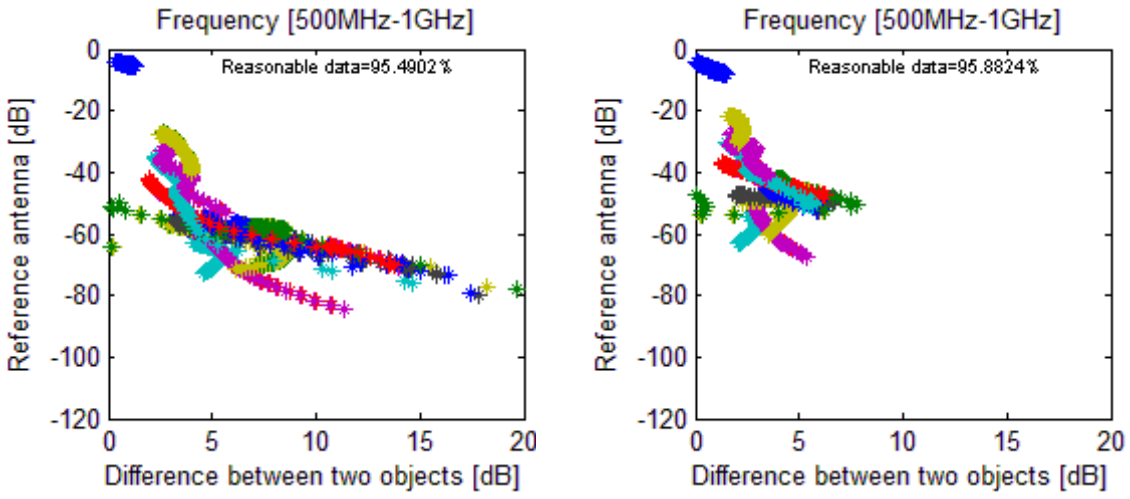

(a) (b)

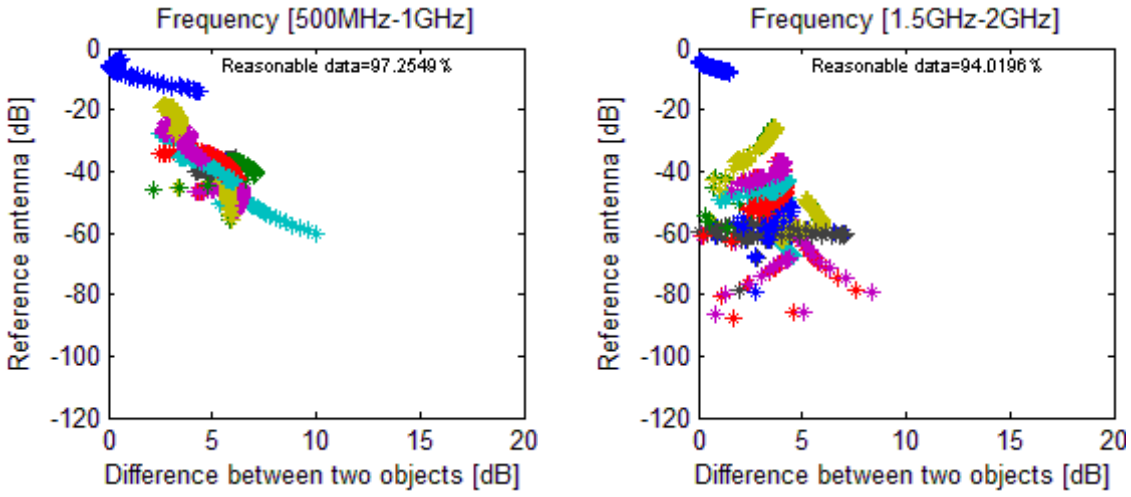

(c) (d)

Figure 14: (a and b) Results of blood and eye phantoms respectively with tumor object of 40mm diameter. (c and d) Two muscle phantoms with tumor object of 40mm diameter.

Figures 15e and 15f show the transmission coefficients of muscle and blood phantoms respectively in the frequency range 500MHz to 1GHz. The results were simulated by using tumor object of 24mm diameter which was placed close to antenna number 1. As expected, the percentage of reasonable data decreased in comparison with figure 14 to become approximately 30% in both phantoms. The transmission coefficient differences between 50℃ and 25℃ have also decreased to the range 0.2 to 3dB. However, the signals are in the range 0 to -60dB which is considered as a strong signal.

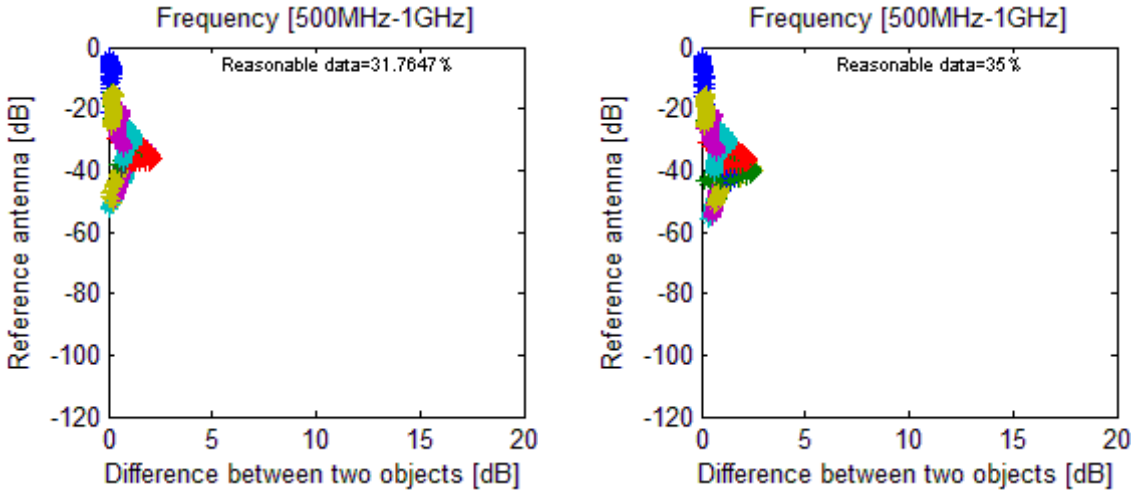

(e) (f)

Figure 15: (e and f) Muscle and blood phantoms respectively with 24mm diameter tumor object.

4.4 Experimental temperature change results and evaluation:

Figures in subtitles 4.4.1 to 4.4.3 highlight a comparison between simulation and measurement results of three different phantoms. The aim is to verify the experimental data in comparison with the simulations under the same conditions. The simulation and measurement setups were performed by using the containers as described in sections 3.2.2 and 3.3 respectively. As described in section 3.4.1, the plots are dividing into three frequency ranges 0.5 to 1 GHz, 1 to 1.5 GHz and 1.5 to 2 GHz. The shown figures in the subtitles are picked up based on the best reasonable data percentage displayed by the three frequency ranges. Other frequency range results are shown in the appendix.

4.4.1 Blood and muscle phantoms including large tumor object in the side:

Figure 16 and 17 show measured and simulated transmission coefficients for blood and muscle phantoms respectively in the frequency range 500MHz to 1GHz. The diameter of the tumor object is 40mm while the outer object is about 100mm. The tumor object is placed in the side close to antenna 1 as shown in figure 6. Figure 16 and 17 show high analogue in the simulation results. This analogue was occurred due to the similarity in the tumors diameter and position. The signal strength of simulations are almost above than -60dB. Further, the transmission coefficient differences are mostly combined in the range 0dB to 2dB. However, S1-6 shows higher differences for blood and muscle phantom. Muscle phantom shows higher percentage of reasonable data in the measurement and simulation results. The percentage of the reasonable data is 12.7% for muscle phantom and 6.8% for blood phantom in the simulation results. Measurement results show 30% for muscle phantom and 17.6% for blood phantom.

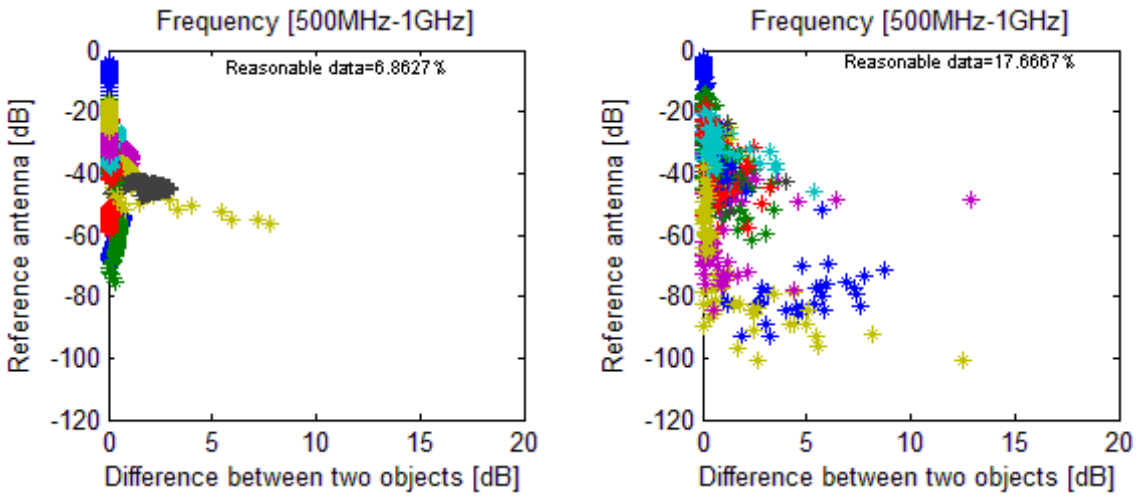

(a) (b)

Figure 16: Blood phantom presents the transmission coefficient differences of 50℃ and 25℃. (a) Simulation result. (b) Measurements results.

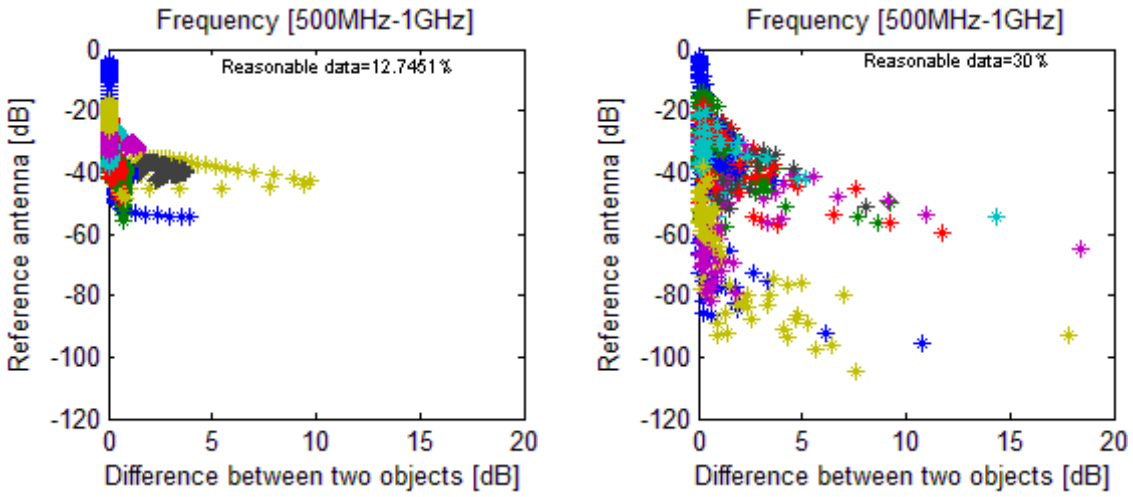

(a) (b)

Figure 17: Muscle phantom presents the transmission coefficient differences of 50℃ and 25℃.
(a) Simulation result. (b) Experimental result.

4.4.2 Muscle phantom including small tumor object in the side:

Figure 18 shows the transmission coefficients for muscle phantom plots in the frequency range 1.5 to 2GHz. The diameters of the tumor and outer objects are 20 and 100mm respectively. The tumor object is placed close to antenna 1. Figure 18a displays the simulation result and figure 18b displays the measurement result. As expected, the reasonable data decreased by reducing the tumor object diameter. The percentage of reasonable data in the simulation result is 12.7% when using a tumor object of 40mm diameter as shown in figure 17a. This percentage decreased to approximately 1% by reducing the diameter to 20mm as shown in figure 18a. However, measurements reasonable data show less decreasing in the percentage as shown in figure 18b. Where the percentage is 28.6% when using 40mm and decreased to only 24% when using 20mm.

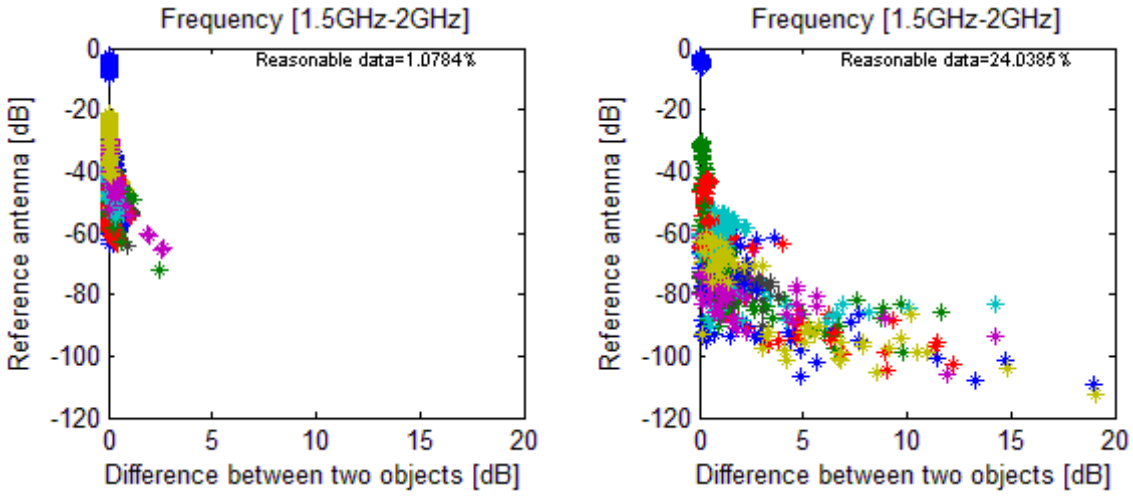

(a) (b)

Figure 18: Muscle phantom plots present the transmission coefficients differences of 50℃ and 25℃.
(a) Simulation result. (b) Experimental result.

4.4.3 Muscle phantom including small tumor object in the center:

Figure 19 shows the transmission coefficient of muscle phantom plots in the frequency range 1 to 1.5GHz. The diameters of the tumor and outer objects are 20 and 100mm respectively. The tumor object is placed in the center of the large phantom. Plot a displays the simulation result and plot b displays the measurement result. The reasonable data of the measurement result shows decreasing in the percentage to become 17.2%. However, simulation's result show a slight increasing to become 5.2%.

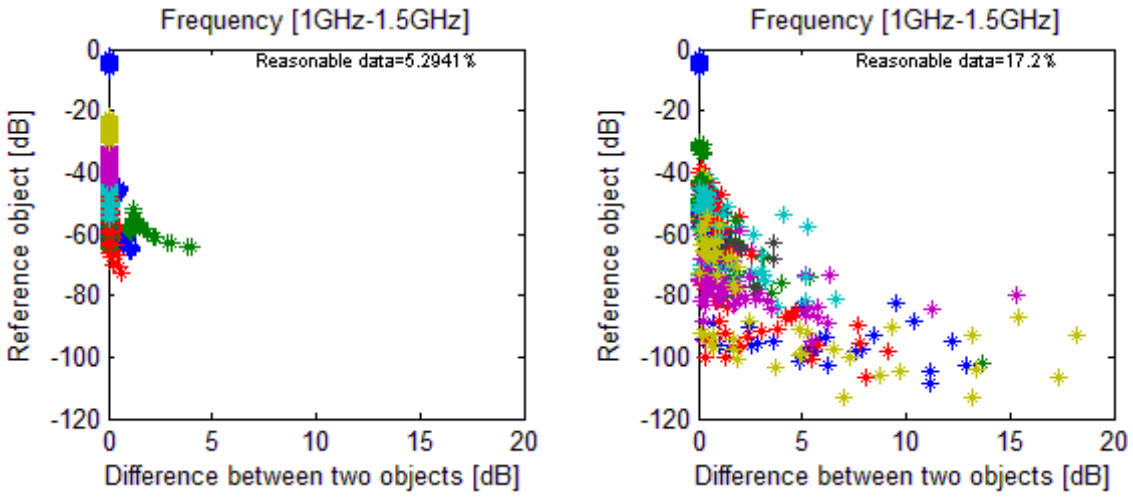

(a) (b)

Figure 19: Muscle phantom plots present the transmission coefficients differences of 50℃ and 25℃. (a) Simulation result. (b) Experimental result.

Measurement results for all three cases in the sections 4.1.1 to 4.4.3 show high analogue among each other as well. Measurement results include more spread signals in comparison with the simulations. Some S matrixes, i.e. S1-8 and S1-13, show weaker signals than others. This occur due to the long distance between these antennas, i.e. 8 and 13, and the tumor object. This long distance cause attenuating in the signal strength to reach the range -85 to -100dB which leads to the noise level. These noise signals cause higher transmission coefficient differences in comparison with other matrixes. Accordingly, all measurement results demonstrate higher transmission coefficient differences in the range of -90dB. This is one reason that can attribute the higher reasonable data in the measurement results. Furthermore, the reasonable data decline in the simulation results can also be attributed to the 2mm weak resolution which was performed in the simulation. This resolution meant that the containers wall and bottom were twice as thick than they are in the lab. This double thickness resulted in the loss of the most radiated part which lead to decreasing the reasonable data.

4.5 Measurements transmission matrix evaluation:

Figure 20 shows different transmission coefficient results of blood and muscle phantoms versus frequency range 0 to 2GHz. The diameter of the tumor object which was simulated and measured is 40mm and is placed close to antenna 1. Simulations and measurements were carried out according to the description in part 3.2.2 and 3.3 respectively. The aim of these plots is to make a transmission coefficient comparsion between simulation and measurement results. The plots demonstrate high transmission coefficient agreements in all frequency ranges for different S matrixes. However, measurement results contains higher noise than simulations especially at frequencies that contain a weak signals around -80dB. Furhtermore, S matrixes which are close to the tumor object, i.e. S11 and S13, demonstrate strong signals in the range -20 to -40dB. However, S matrixes which represent antennas in the opposite side, i.e. S1-10 and S6-14, show weaker signals in the range -80dB.

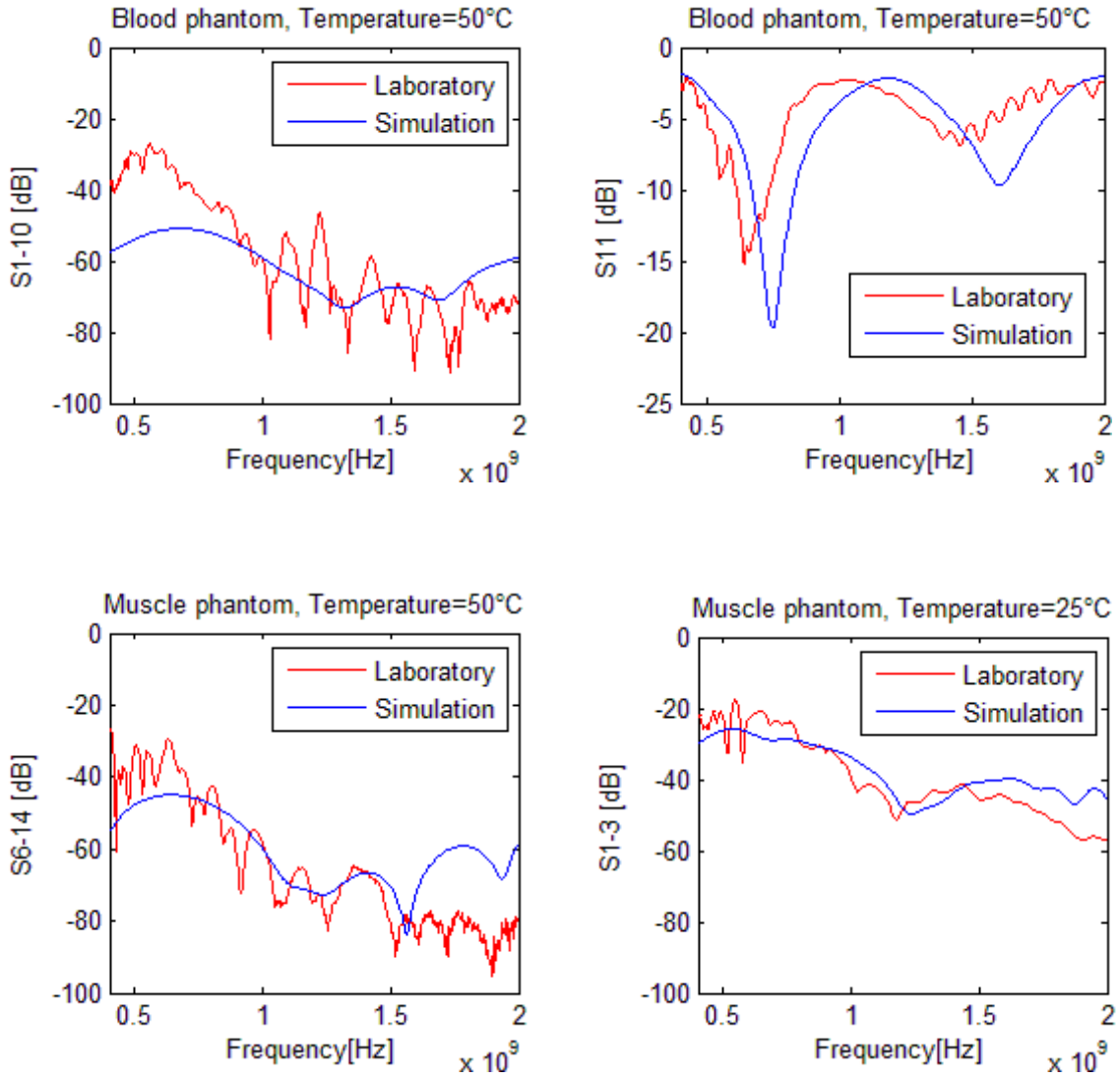

Figure 20: Different phantom plots demonstrate the transmission coefficient similarity between measurement and simulation results. The temperature in the title represents the tumor object temperature.

4.6 Closer antenna array:

The aim of this part is to reveal the behavior of transmission coefficients by implementing antenna array which is closer to the phantom. The idea of the closer array came since the advent of the results which showed transmission coefficients differences between two various temperatures less than 1dB. The simulations were carried out according to the description setup in section 3.2.2 except the antennas coordinates which are 30% closer than the normal array as indicated in figure 21a. Implementing antennas array, which is closer to the phantom, provided higher energy as well as a stronger signal. Figure 21b demonstrates the effectiveness of the closer array on the signal strength, where it provided 20dB stronger signal.

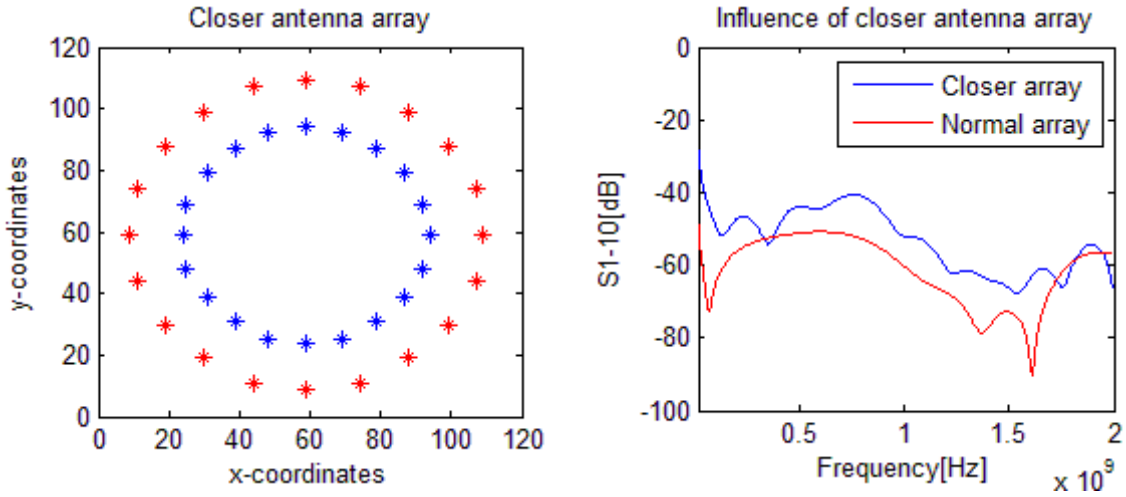

(a) (b)

Figure 21: (a) Closer and normal antenna arrays coordinates. (b) Comparing between two S1_10 matrix under same conditions for normal and closer array.

4.8 Sensitivity to tumor spot diameter:

Figure 22 represents a summary of the simulation results which highlights the relation between the tumor diameter versus the percentage of reasonable data. For instance, 42mm diameter of tumor object shows 91.6% of reasonable data for muscle phantom. This figure can be considered as one of the important goals in this thesis. Where it indicates the feasibility of the antennas system to estimate the temperature changes of five different diameters. Figure 22a demonstrates the relation without using the containers while figure 22b shows the results by using the containers. Figure 22a shows system's potential to successfully estimate the temperature changes when the tumor diameter is 32mm or larger. The figure shows that 32mm can be considered as the boundary between the accepted and unaccepted results. Where the percentage at this diameter is 60% which a good result, whilst at 24mm diameter the percentage decreased to approximately 20% which is too low.

Figure 22b demonstrates the effectiveness of the containers on the results. Where the 42mm diameter shows only 12% of reasonable data. Which implies that the system is unable to successfully track the temperature changes by using this type of containers.

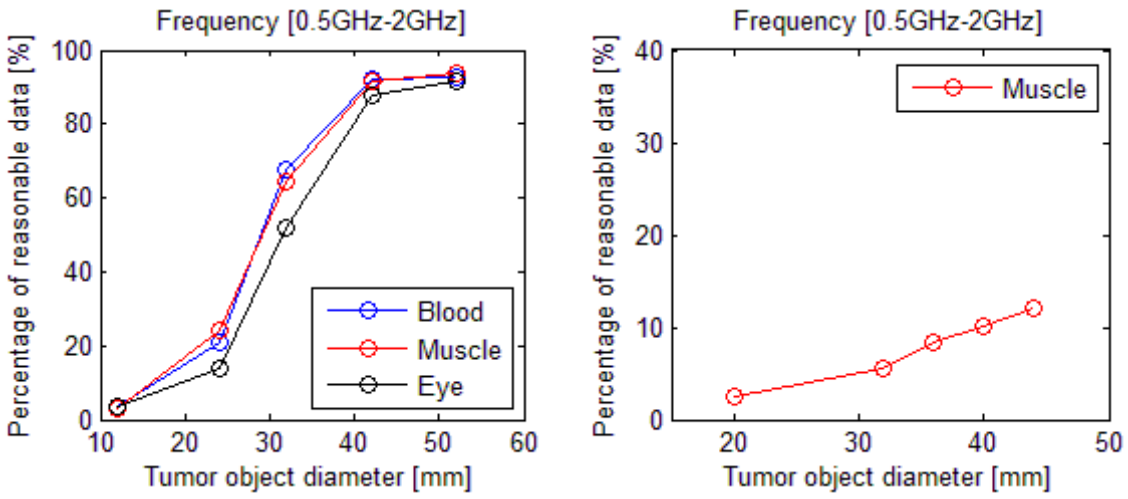

(a) (b)

Figure22: The relation between tumor object diameter and percentage of reasonable data. (a) Simulation results without using container. (b) Simulation result when using containers.

4.9 Sensitivity to temperature tracking:

Figure 23 shows the relation between different temperature tracking degrees versus the percentage of reasonable data. For instance, 15℃ tracking means 50℃ -35℃ or 40℃ - 25℃. The figure shows simulation result without using the containers. The tumor object diameter is 42mm. The importance of figure 23 is to estimate the feasibility of the antennas system to track small temperature changes. The most important temperature tracking range is between 37℃ and 43℃ which represents the range that is actually used during hyperthermia treatment. This hyperthermia range represents 6℃ tracking change. Figure 23a demonstrates systems potential to successfully estimate 10℃ where the percentage of reasonable data is about 82%. However, a significant decline appeared at 5℃ tracking where the percentage is approximately 25%.

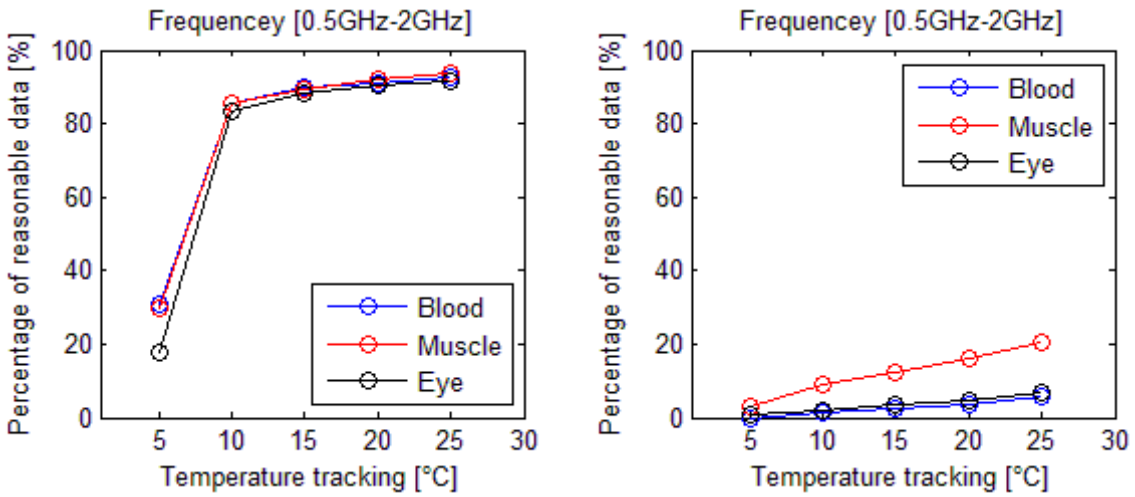

(a) (b)

Figure 23: The relation between different temperature tracking degrees and percentage of reasonable data. (a) Tumor spot is placed close to the wall. (b) Tumor spot is placed in the center.

5

Discussion

The temperature dependence of the permittivity showed analogue in the slope of blood and eye phantoms at 1.02GHz in figure 11. The permittivity of blood and eye phantoms decreased with 0.7% and 0.67% per 1℃ respectively. While the permittivity of muscle phantom decreased with 0.42% per 1℃. This can be attributed to the salt concentration in each phantom, where the blood and eye phantoms include 1.2% salt whilst there is only 0.6% in the muscle phantom. However, the conductivity of muscle and eye phantoms increased with 0.27% and 0.304% per 1℃ respectively. While the blood phantom demonstrated a larger increasing with 0.606% per 1℃.

The results generally can be divided in two main parts. The first part without using the containers and second part with the containers according to the description in sections 3.2.2 and 3.3 respectively. The results in the first part showed a high possibility to monitor the temperature distribution when using tumor object diameter in the range of 32mm and higher. Where the reasonable data reached high percentage up to 97% as indicated in figure 22a. However, the second part was simulated and measured by using the containers. A significant decline was demonstrated in the second part where the percentage range of the reasonable data became approximately 20% as indicated in figure 22b. The simulation and measurement results in the second part showed however good analogue in the reasonable data percentages.

5.1 Relation between antennas and objects position:

A worthwhile issue which was generally observed in all results is the relation between the position of the tumor object and the antennas. For instance, if the tumor object is located close to antenna number 1, then all S matrixes in these sections (e.g. S1_2) has the ability to show a stronger signal and higher transmission coefficient differences [dB] between two various temperatures than the matrixes in the other side (e.g. S1_13) as described in figure 6. This is due to the short distance between the antenna number 1 and the tumor object, which prevents the loss of the microwaves concentration and strength. However, the antennas on the opposite side are suffering from the long distance which leads to loss of microwaves concentration. Figure 24 demonstrates a simulation example of this relation, where a blood phantom was used and the tumor object was placed in the side close to antenna 1. This simulation example was performed without using containers. Plot 24a displays the signal strength of S1_2 where the stars assembly are placed approximately at -40dB. Plot 24b demonstrates the signal weakness of S1-13 where the stars assembly is placed at -70dB which represents a weak signal. Moreover, the transmission coefficient differences [dB] between two various temperatures of S1_2 are in the range 3 to 6dB while it's lower than 3dB in S1-13.

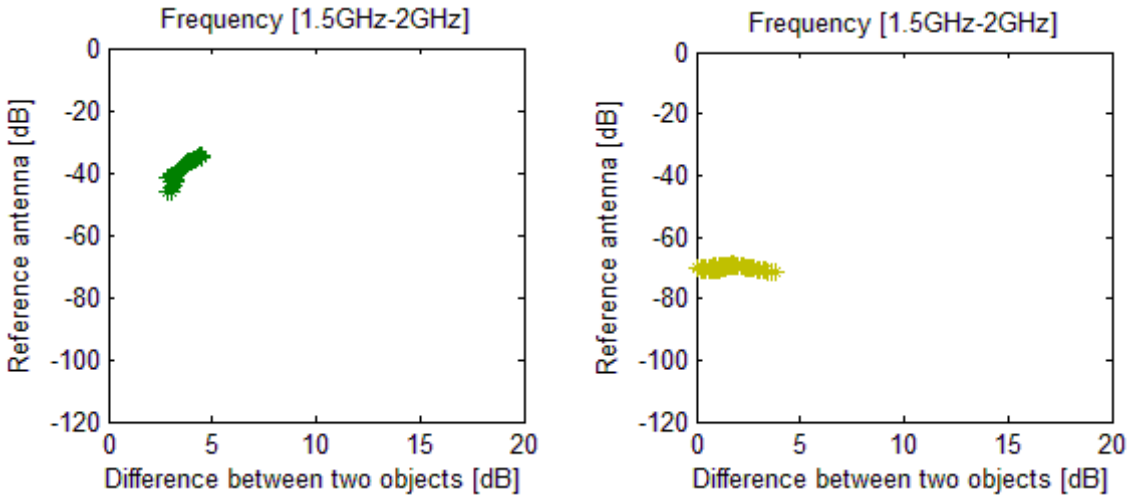

(a) (b)

Figure 24: Temperature differences of two different S matrixes. Plot (a) S1-2 which is close to the heated object. (b) S1-13 which is far from the heated object.

Accordingly, all results which were performed with the tumor object in the center showed a decline in the reasonable data percentage comparing with those placed close to the wall. Figure 23b demonstrates this decreasing, where the temperature tracking accuracy of 25℃ resulted in only 25% reasonable data when the tumor object is placed in the center. Whilst it displayed high percentage up to 95% when the tumor object is placed close to the wall as shown in figure 23a.

5.2 Sensitivity of tumor spot diameter:

The diameter of the internal tumor is the most influential factor in the results. In all results, the percentage of the reasonable data increase when the tumor diameter becomes larger. Which implies that the transmission coefficient difference between two various temperatures and the signal strength become higher. This observation is clearly shown in figure 22, where the percentage of the reasonable data is around 60% when the tumor diameter is 32mm. Moreover, the percentage increase up to 95% at 52mm diameter. However, results at 24mm displayed a significant decline in the reasonable data to only 20% which implies that low diameters are still a challenging case for the microwave system.

5.3 Compatibility between simulations and experiments:

The transmission coefficients in figure 20 demonstrates high agreement between simulation and measurement results in the frequency ranges 0 to 2GHz. Moreover, the overall shape of plots stars in section 4.4 shows in some extent good agreement between measurements and simulations results. For instance, the stars assembly in figure 18 shows a triangle shape in the measurement and simulation results. However, in all cases measurement results demonstrated approximately 13% higher reasonable data than simulations. Which implies that the transmission coefficient differences between two various temperatures in the measurement results are higher than simulations. This percentage difference between simulation and measurement results can be attributed to many reasons. The most obvious reason is that some S matrixes, i.e. S1-8 and S1-13, show weaker signals than others. This occur due to the long distance between these antennas, i.e. 8 and 13, and the tumor object. This long distance cause weakness in the signal strength (-85dB) which lead to the noise signals. These noise signals cause higher transmission coefficient differences in comparison with other matrixes. Accordingly, all measurement results demonstrate higher transmission coefficient differences in the range of -90dB. Other reason that can attribute the difference is the implementing of weak resolution in the simulations setup which was 2mm due to the scope of this study. This resolution meant that the containers wall and bottom were twice as thick than they are in the lab. This double thickness in the simulation resulted in the loss of the most radiated part. Thus the reasonable data percentages become lower. Finally, the percentage difference between simulations and measurements results can also be attributed to the calibration error in the lab which certainly cannot happen in the simulation.

5.4 Influence of closer antenna array:

Results in figure 21b demonstrated the effectiveness of closer antenna array on the signal strength. Where closer antenna array data showed approximately 20dB stronger transmission coefficients signal than the normal array.

Moreover, figure 24 displays a simulation results example of muscle phantom including small tumor object placed in the center. Plot 24a shows normal antenna array results while plot 24b shows closer array results. Plot 24b demonstrates the improvement of closer array where the reasonable data increased from 21.6% to 37.2%. This percentage implies that the transmission coefficient differences [dB] between two various temperatures become higher. Accordingly, the closer array can be an appropriate solution to the results which displayed low [dB] differences between various temperatures.

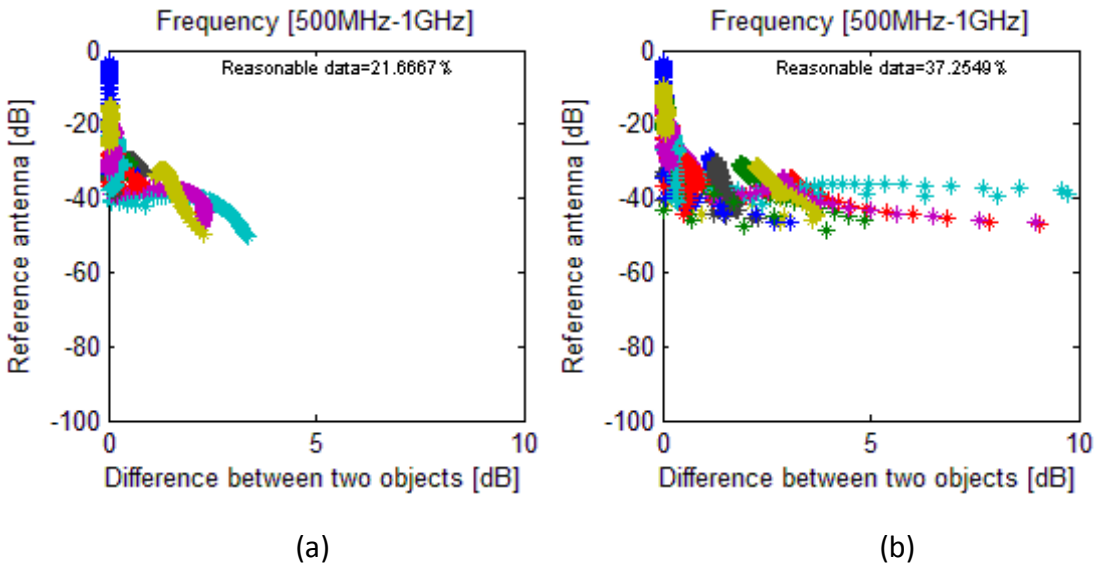

(a) (b)

Figure 24: Muscle phantom with tumor object inserted in the center. (a) Normal antenna array. (b) 30% closer antenna array.

5.5 Influence of the containers:

The aim of performing containers simulation was to simulate the same experimental model to verify measurement results as indicated in section 3.2.2. The containers wall and bottom, each 1mm thick, have a significant impact on the measurement and simulation results. Section 4.3 which was simulated without using the containers displayed high reasonable data percentages in comparison with the results in section 4.4 which was measured and simulated by using the containers. Moreover, figure 25 displays the significant effectiveness of the containers, where it demonstrates several tumor object diameters versus the percentage of the reasonable data. It is clearly shown that the reasonable data decreased from 91% without using the containers to 12% with the containers when the tumor object diameter is 42mm. This dramatic decline may be attributed to the containers type which have permittivity and conductivity of 2.2 and 0.07s/m respectively. Whilst water's permittivity and conductivity are 78 and 0.1s/m respectively. This huge difference between the waters and containers dielectric properties triggered the loss of the electromagnetic coupling which caused the reflection of the antennas waves.

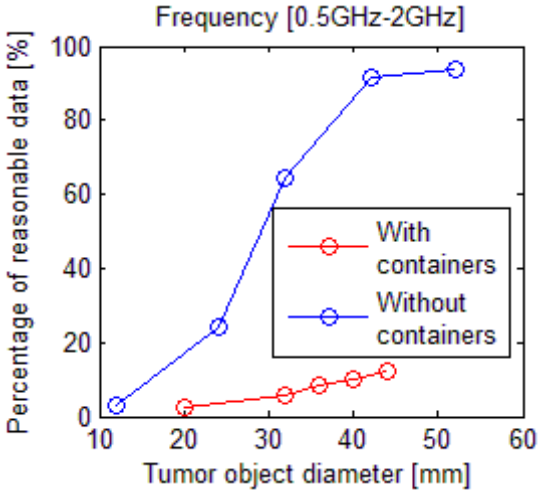

Figure 25: The influence of the containers on the percentage of the reasonable data.

5.6 Estimate small temperature change tracking:

Sections 4.3 and 4.4 present several temperature tracking results which represent the range between 25℃ and 50℃ that may be considered as an ideal range. However, the most important temperature tracking range is between 37℃ and 43℃ which represents the range that is actually used during hyperthermia treatment. This hyperthermia range represents 6℃ tracking change. Figure 26a demonstrates systems potential to successfully estimate temperature tracking of 10℃, where the percentage of reasonable data reached 82%. However, a huge decline occurred in the temperature tracking of 5℃ which results only in 25%. This implies that the current simulation setup still require more improvements in order to successfully estimate small temperature tracking ranges such as 5℃.

However, all percentages of reasonable data in this thesis were calculated based on two constant thresholds as described in section 3.4.1. These two thresholds have high effectiveness on the reasonable data values. Accordingly, these thresholds have a significant impact on the temperature tracking accuracy of 5℃ as shown in figure 26a. Where the highest percentage value for 5℃ tracking reached 30%. Any modification in the threshold values will certainly affect the reasonable data percentage. Other test was performed by reducing one of these thresholds which is the interval value between two various temperatures [dB]. This threshold was reduced from 1dB to 0.7dB. This threshold modification means that all frequencies (i.e. stars) which are higher than 0.7dB are calculated within the percentage of reasonable data. Figure 26b displays the effectiveness of this modification on the percentage of reasonable data. Where the temperature tracking accuracy of 5℃ showed accepted percentage up to 78%. It's shown how this threshold plays a significant role in the temperature tracking accuracy.

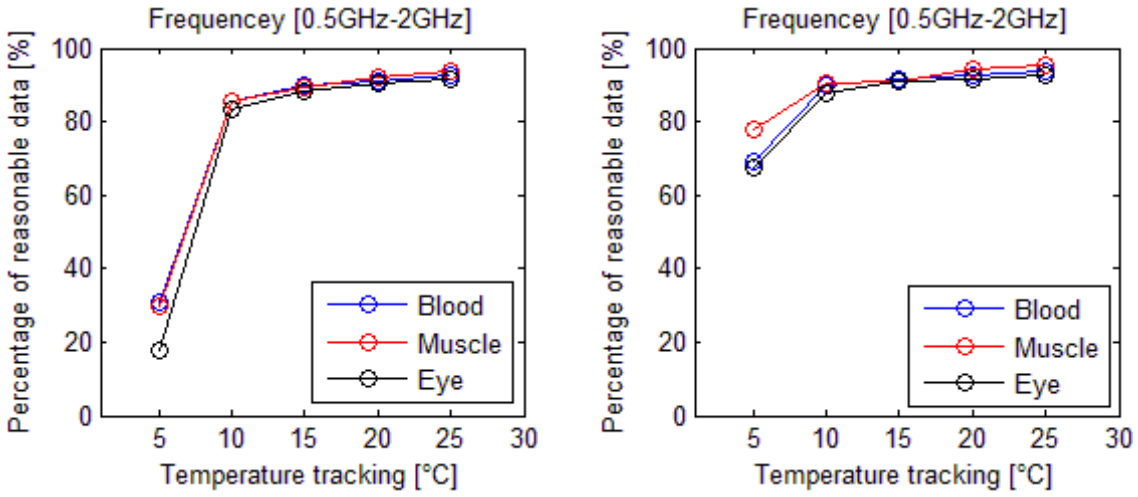

Figure 26: Different temperature tracking degrees versus the percentage of the reasonable data. (a) Normal thresholds as described in section 3.4.1. (b) Reducing the threshold from 1dB to 0.7dB

Meaneys group performed number of studies which are related to this thesis [20]. Their results demonstrated the ability to track the temperature difference around 0.2℃. This is in contrast to the results presented in this thesis which showed that it is difficult to achieve this high tracking accuracy. This can be attributed to some of their experimental setups which provided their better results. Their tumor object diameter was 51mm which is approximately similar to the diameter that is used in this thesis. Further, they employed 32 monopole antennas placed in array of 15cm. Whilst in this thesis it is 20 monopole antennas placed in array of 20cm. Moreover, their data were collected at 9 frequencies in the range 300 to 700MHz. Whilst the data in this thesis were extracted at wide frequency range from 500MHz to 2GHz. These setup differences have a positive affect on their results.

However, the most crucial factor is seemingly the acceptable threshold level. In this thesis we defined the reasonable data based on the 1dB threshold as described in section 3.4.1. In light of results of meaneys group, this threshold seems to be too strict. However, this 1dB value is just an assumption which was selected as an initial appropriate value to determine the reasonable data percentages. Figure 26b demonstrates the effectiveness of reducing this threshold from 1dB to 0.7dB. The percentage of reasonable data increases when the threshold [dB] becomes lower. However, the exactly appropriate threshold value can be defined as the lowest value which results in an acceptable tracking image. The importance of this lowest threshold value is to accurately determine the feasibility of the microwave system to estimate its sensitivity to small temperature changes. For instance, to determine the feasibility of the microwave system to tracking small temperature tracking changes such as 5℃.

This lowest acceptable threshold cannot be decided before image reconstruction implementation. If the reconstructed image shows that for instance 0.5dB is an adequate threshold value, then it is possible to track the temperature distribution in the image. In the case that the reconstructed image proved the possibility to track the temperature changes when using threshold lower than 1dB, then all results which showed low reasonable data percentages will greatly improve. Moreover, a significant improvement will occur in the temperature tracking accuracy of 5℃ as displayed in figure 26b. Moreover, the improvement may also occur on the temperature tracking of 1℃. However, if the reconstructed image showed that it is not possible to track the temperature changes when using threshold lower than 1dB, then the temperature tracking of 5℃ is still a challenging case of the microwave system. Accordingly, it is necessary that the image reconstruction process should be a prioritized initial step in future work.

6

Conclusion

The aim of this thesis was to determine the feasibility of using microwave thermal imaging to estimate its sensitivity to temperature changes. The advantage of this system is that the same antenna array can be simultaneously used in thermal imaging and hyperthermia treatment. Generally, some cases showed good results while others still need improvements to give better results. For instance, tumor objects which are existing close to the wall showed results more convincing than those existing in the center. Moreover, tumor object diameter was one of the most important factors that affects the results. In the sense that the larger diameter shows higher percentage of reasonable data. The boundary between acceptable and unacceptable results is 32mm diameter for tumor object without using the containers. Certainly, the diameters above this boundary results in higher reasonable data up to 97%. While lower diameters such as 24mm demonstrated approximately 20% only. In addition, the system could successfully estimate the temperature tracking of 10℃ which showed high percentage up to 83%. However, the most important temperature range for hyperthermia treatment is between 37℃ and 43℃ which still a challenging step in case of using 1dB threshold. However, if we assumed that 0.7dB is an adequate threshold, then 5℃ temperature tracking change showed acceptable results.

Results which were obtained by using the containers demonstrated a significant decline in the reasonable data. Certainly, the main reason of this decline is the containers bottom and wall, where the most radiated waves are loss. The results showed a good transmission coefficients agreement between simulations and experimental results. However, simulation results showed lower percentage of reasonable data than experimentals. This difference can be attributed to the 2mm weak resolution which has been performed in the simulation.

7

Future Work

Results give an incentive to work forward in this area and perform broader and more accurate studies. Future work can be performed in different areas, whether in the phantom or in the system itself. First issue to be inquired is the implementation of image reconstruction in order to determine the adequate threshold [dB] value between two various temperatures as described in section 5.6.

The temperature dependence of dielectric properties results demonstrated different slope degrees on each frequency. The measurements and simulations in this thesis were performed based on the dielectric properties values at 500MHz. Moreover, other frequency values that can be implemented, e.g. 1GHz, may provide higher dielectric properties change than 500MHz. New issue to be inquired is testing phantoms which are more realistic. For instance, heating more than one tumor spot at different positions. Also, heat tumor phantom type which differs from the whole object. For instance, using muscle phantom as a tumor spot and blood phantom for the large phantom. Moreover, using containers with appropriate dielectric properties may provide higher electromagnetic coupling. Further, using containers with thinner wall and bottom will probably reduce the containers adverse effect on the results. Other tricky point is the liquid phantoms which were using in this thesis. This liquid phantoms suffer from changing its dielectric properties suddenly. Which enforced us to perform new phantoms continuously, thus reduced the number of measurements. Moreover, liquid phantoms require containers which were the main reason of reasonable data significant decline. Consequently, solid phantoms can be implemented instead of liquid ones which don’t require containers. Thus, number of measurements can increase as well as getting more accurate and realistic results.

Monopole antennas which were utilized in this thesis are simplest antenna type. Any other antenna type such as directional antennas may improve the results. The advantage of the directional antenna is that it radiates the microwaves in a specific direction which provides higher energy than monopole antennas that radiates everywhere. Furthermore, using two or three antenna arrays with eight antennas in each ring instead of using one ring with twenty antennas may results in more prevalent waves as illustrated in figure 27.

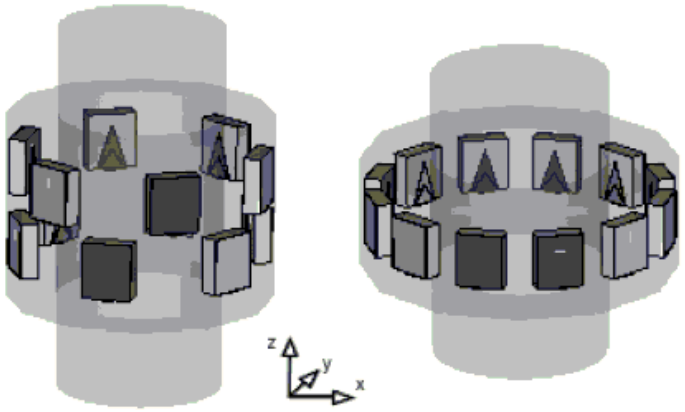

(a) (b)

Figure 27: Two different antenna arrays setups. (a) Antenna arranged in two arrays while in (b) it's arranged in one array like the one used in this thesis (2).

Bibliography

[1]Statistics: Cancer in Sweden 2012, http://www.cancerfonden.se/

[2] H. Trefna, Advances in microwave hyperthermia treatment using time reversal, Thesis for the degree of Doctor of Philosophy.

[3] Cabury, E. "Hyperthermia in Cancer Treatment." pp. 1-48, 2011

[4] Medical center cologne, http://www.medical-centercologne.com/therapies/local-hyperthermia/

[5]M. R. Anglin, "what are the different types of hyperthermia treatment?", 2003, http://www.wisegeek.com/what-are-the-different-types-of-hyperthermia-treatment.htm

[6] R. M. ARTHUR, W. L. STRAUBE, J. W. TROBAUGH, & E. G. MOROS, "Non-invasive estimation of hyperthermia temperatures with ultrasound", Int. J. Hyperthermia, pp. 589-600, 2005

[7] Yasutoshi Ishihara, Naoki Wadamori and Hiroshi Ohwada (2010). Non-invasive Localized Heating and Temperature Monitoring based on a Cavity Applicator for Hyperthermia, New Developments in Biomedical Engineering, Domenico Campolo (Ed.), ISBN: 978-953-7619-57-2, InTech.

[9] F. M. WATERMAN, "invasive thermometry techniques", pp. 331-358, 1995.

[10]Peter Wust, Johanna Gellermann, "Regional Cancer Therapy", pp. 73-88, 2007 http://books.google.se/books?id=dQw2sACha8C&pg=PA73&lpg=PA73&dq=Regional+and+partbody+hyperthermia&source=bl&ots=cwjqEydJvo&sig=lF5l_7vhCffsvxQ6WrCItFC0HVU&hl=en&sa=X&ei=2ARYUd3OEjk4QTu0oBg&ved=0CGYQ6AEwCQ#v=onepage&q=Regional%20and%20part-body%20hyperthermia&f=false

[11] Lutz Ludemann, Waldemar Wlodarczyk, Jacek Nadobny, Mirko Weihrauch, Johanna Gellermann and Peter Wust, "Non-invasive magnetic resonance thermography during regional hyperthermia", Int. J. Hyperthermia, pp. 273-282, 2010.

[12] B Hildebrandt, G Streenivasa, B Rau, J Gellermann, H Riess, R Felix, PM Schlag, "Hyperthermia in combined treatment of cancer", Volume 3, pp. 487-497, 2002. http://www.sciencedirect.com/science/article/pii/S1470204502008185

[13]Agilent Technologies, “Basics of measuring the dielectric properties of materials”, 2006.

[14] “Luxtron 755 Multichannel Fluoroptic Thermometer”. http://www.torontosurplus.com/industrial/gauges-readouts-counters/luxtron-755-multichannel-fluoroptic-thermometer.html

[15] V. Rieke and K.B. Pauly, “MR thermometry”, J. Mag. Res. Imag., vol. 27, pp.376-390, 2008.

[16]M. Miyakawa, “Tomographic Measurement of Temperature Change in Phantoms of the Human Body by Chirp Radar-Type Microwave Computed Tomography”, pp. 31-36, 1993.

[17] J.C. Bolomey, L. Jofre, G. Peronnet, “On the possible use of microwave-active imaging for remote thermal sensing”, vol. MTT-31, pp. 777-781, 1983.

[18] M. Helbig, K. Dahlke, I. Hilger, M. Kmec, J. Sachs, “UWB microwave imaging of heterogeneous breast phantoms”, pp. 486-489, 2012.

[19] H. Trefna, A. Fhager, J. Hellman, M. Persson, “Microwave theremal imaging: towards hyperthermia”, pp. 1-11, 2010.

[20] P.M. Meaney, K.D. Paulsen, M.W. Fanning, D. Li, Q. Fang, “Image accuracy improvements in microwave tomographic thermometry: phantom experience”, Int. J. Hyperth, vol. 19, pp. 534-550, 2003.

[21] P.M. Meaney, M.W. Fanning, K.D. Paulsen, D. Li, SA Pendergrass, Q. Fang, KL Moodie, ”Microwave thermal imaging: initial in vivo experience with a single heating zone”, Int. J. Hyperth, vol. 19, pp. 617-641, 2003.

[22] P.M. Meaney, T. Zhou, M.W. Fanning, S.D. Geimer, K.D. Paulsen, “Microwave thermal imaging of scanned focused ultrasound heating: phantom results”, Int. J. Hyperth, vol. 24, pp. 523-536, 2008.

A

Appendix

A.1: Simulations and measurements difference results:

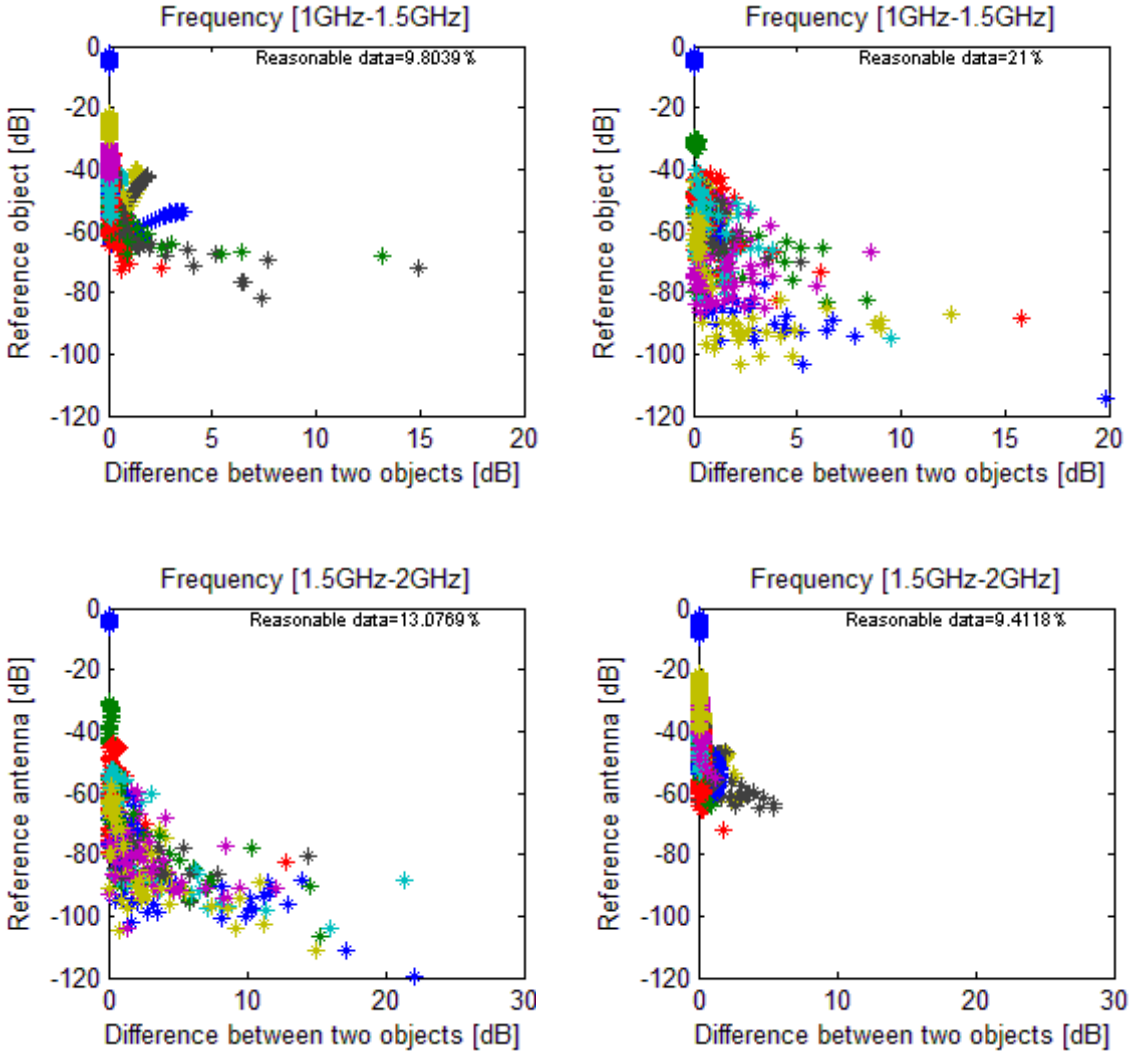

(a) (b)

Figure A.1: Muscle phantom plots including 40mm diameter tumor object close to antenna 1. Plots represent the difference between 50℃ and 25℃. (a) Simulation results. (b) Measurements results.

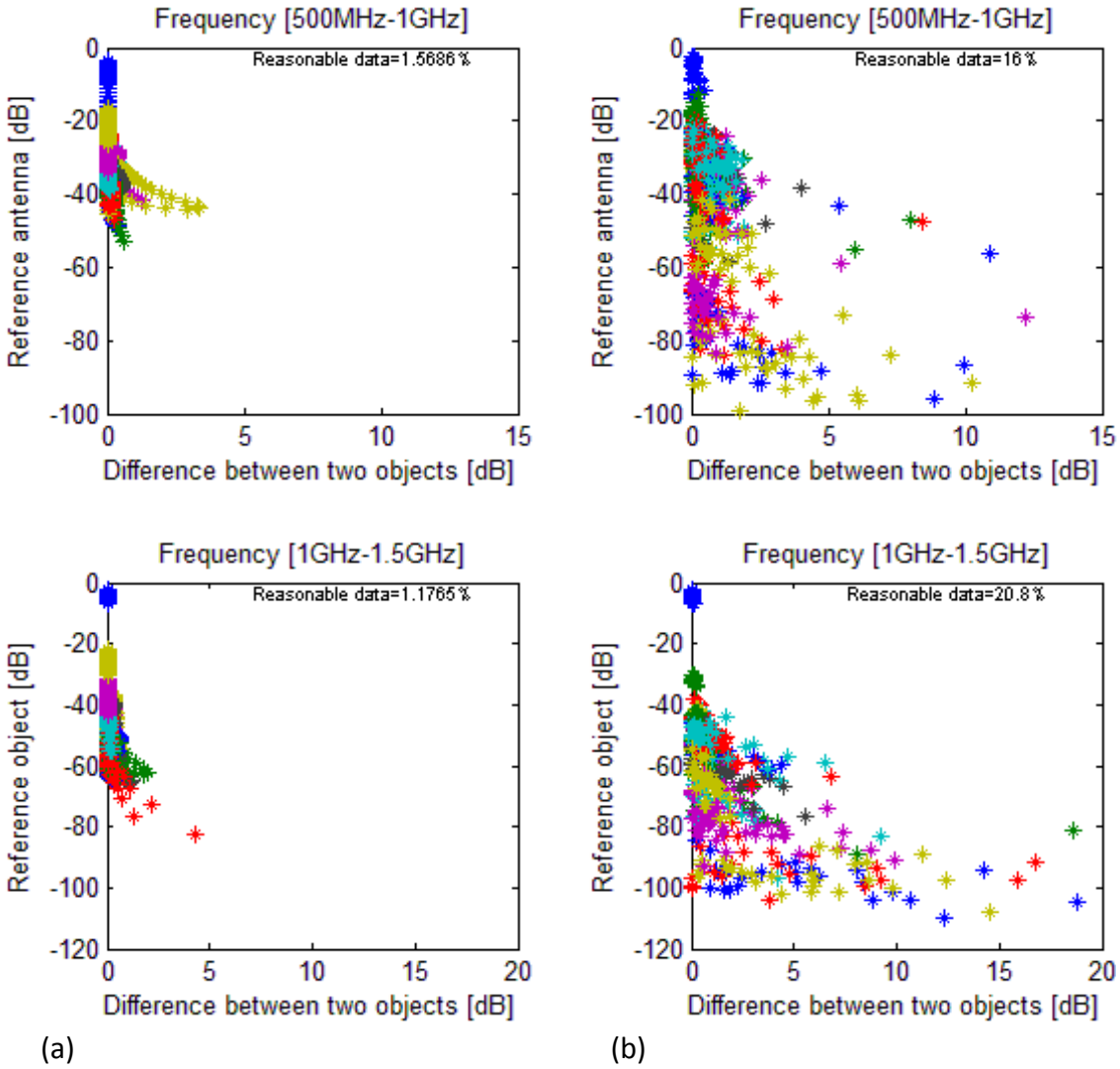

Figure A.2: Muscle phantom plots including 20mm diameter tumor object close to antenna 1. Plots represent the difference between 50℃ and 25℃. (a) Simulation results. (b) Measurements results.

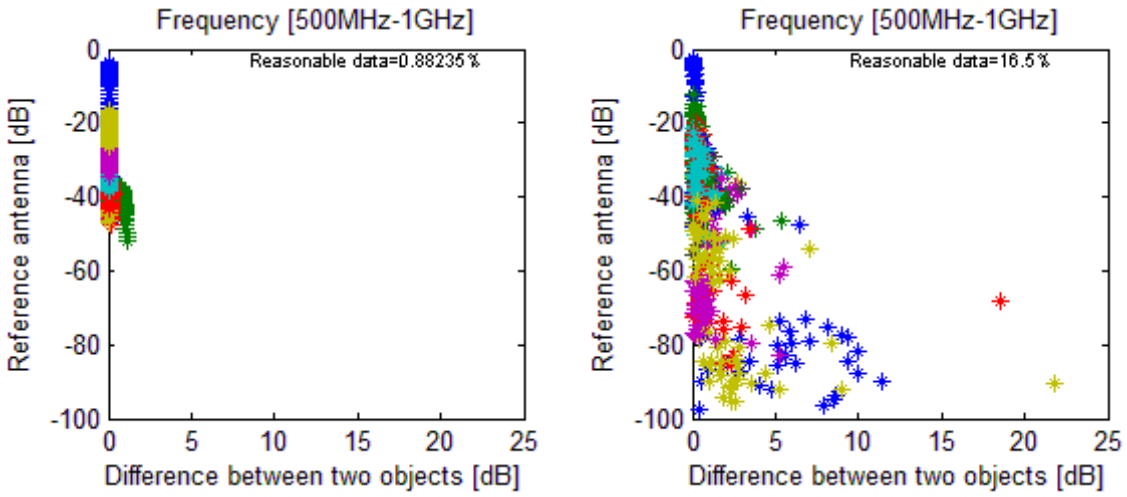

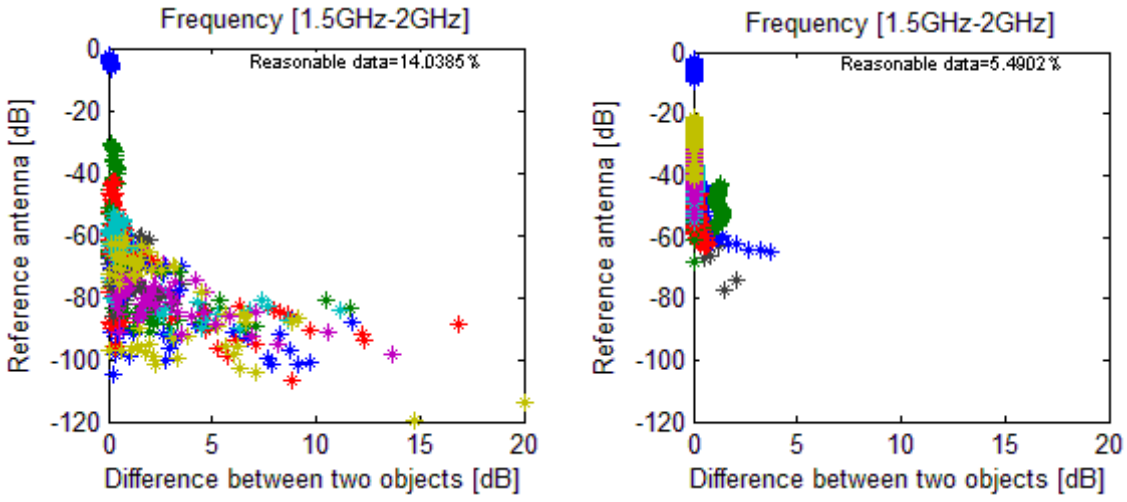

(a) (b)

Figure A.3: Muscle phantom plots including 20mm diameter internal object in the center. Plots represent the difference between 50℃ and 25℃. (a) Simulation results. (b) Measurements results.

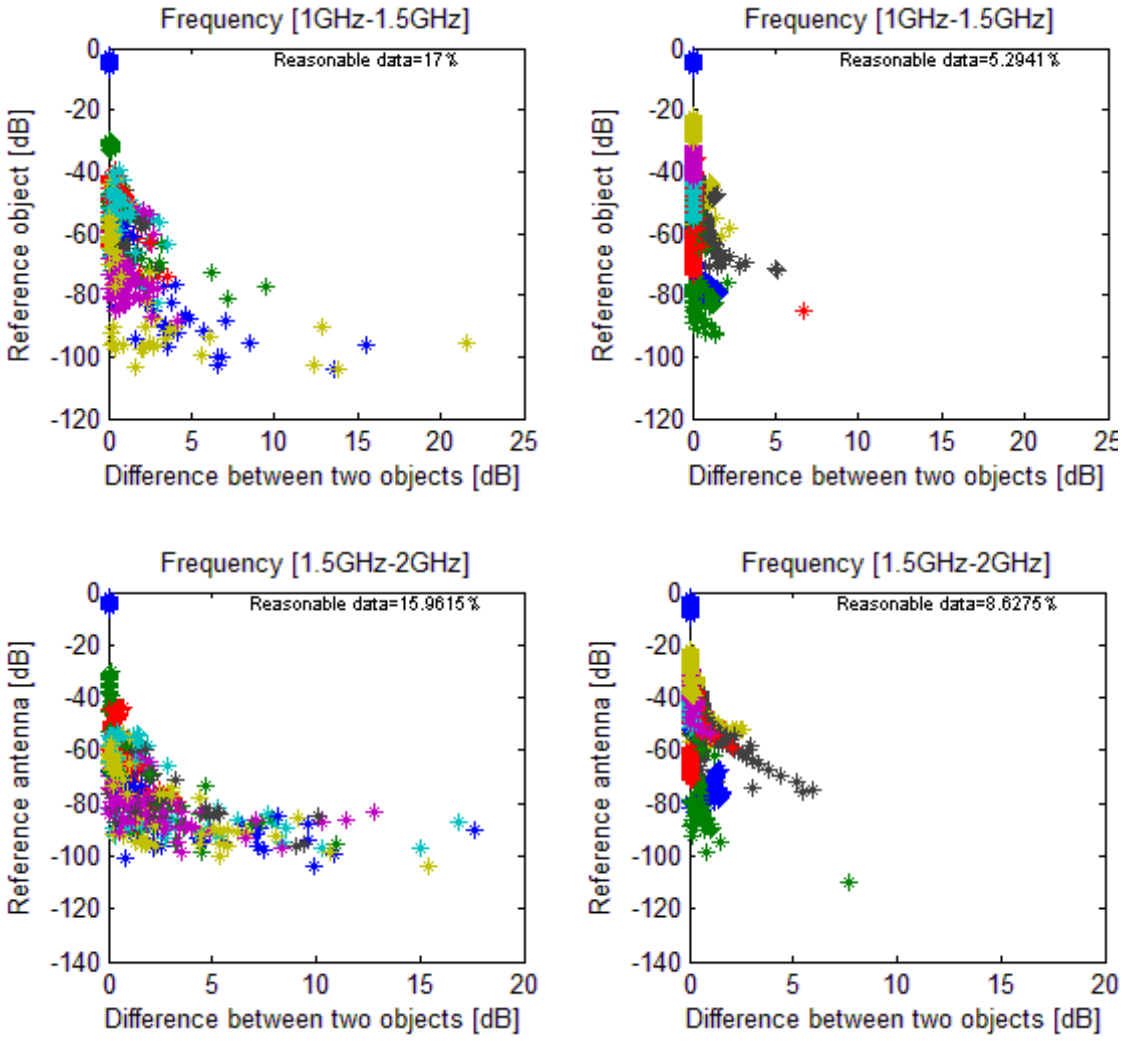

Figure A.3: Blood phantom plots including 40mm diameter tumor object close to antenna 1. Plots represent the difference between 50℃ and 25℃. (a) Simulation results. (b) Measurements results.

A.2 Simulations and measurements transmission coefficients matrix results :

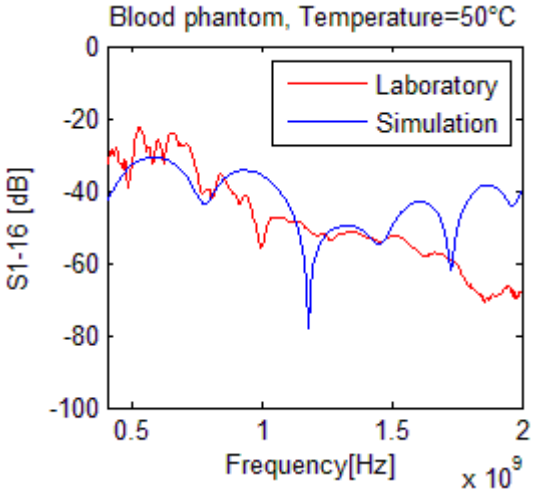

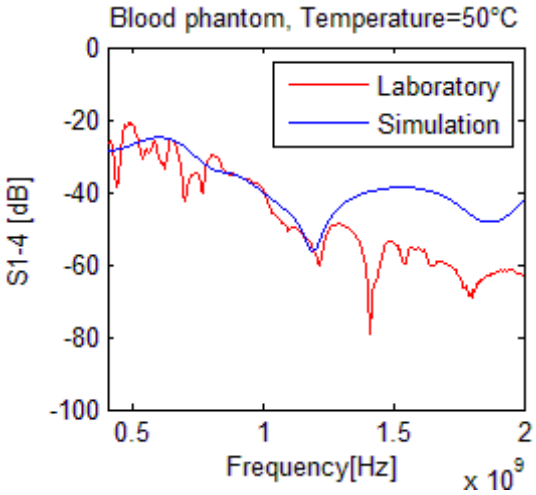

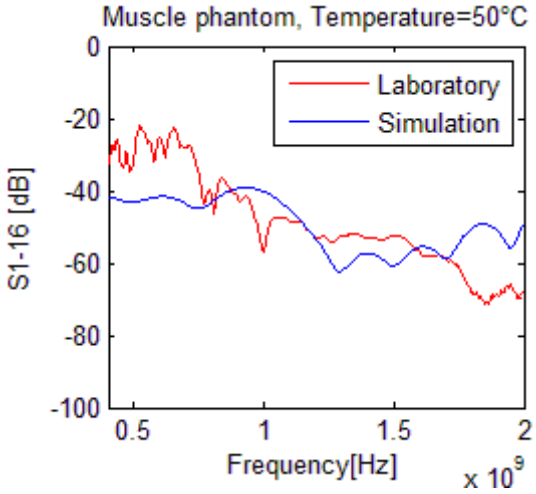

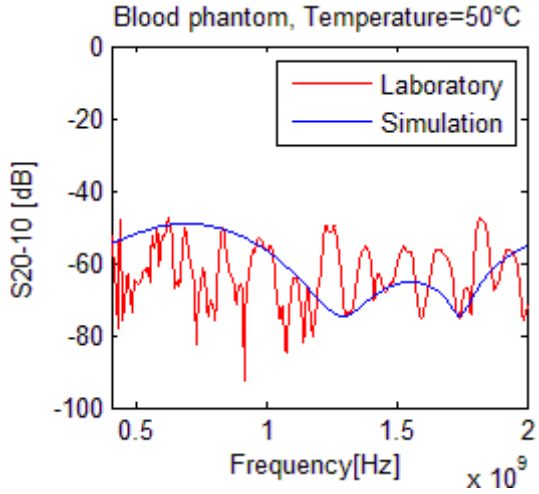

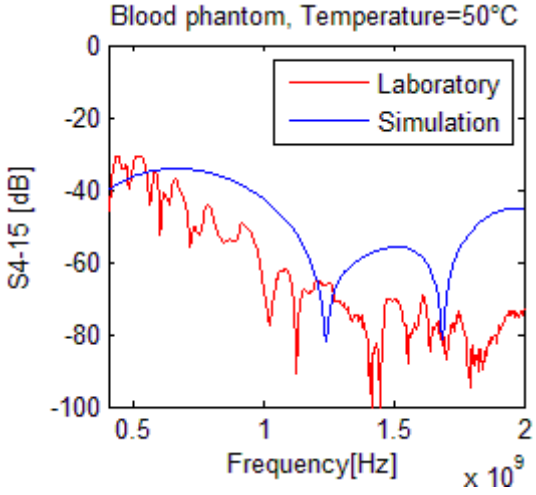

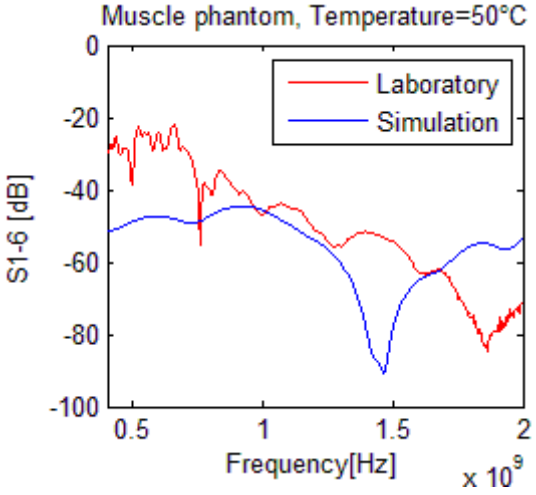

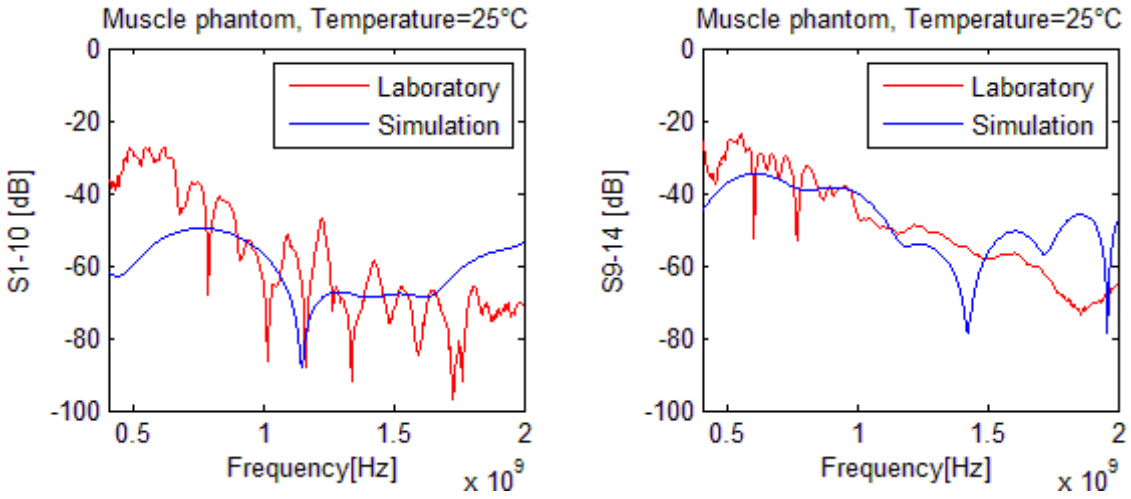

Figure A.4: Different phantom plots show the compatibility between measurement and simulation results. The temperature in the title represents the tumor object temperature with 40mm diameter located close to antenna 1.

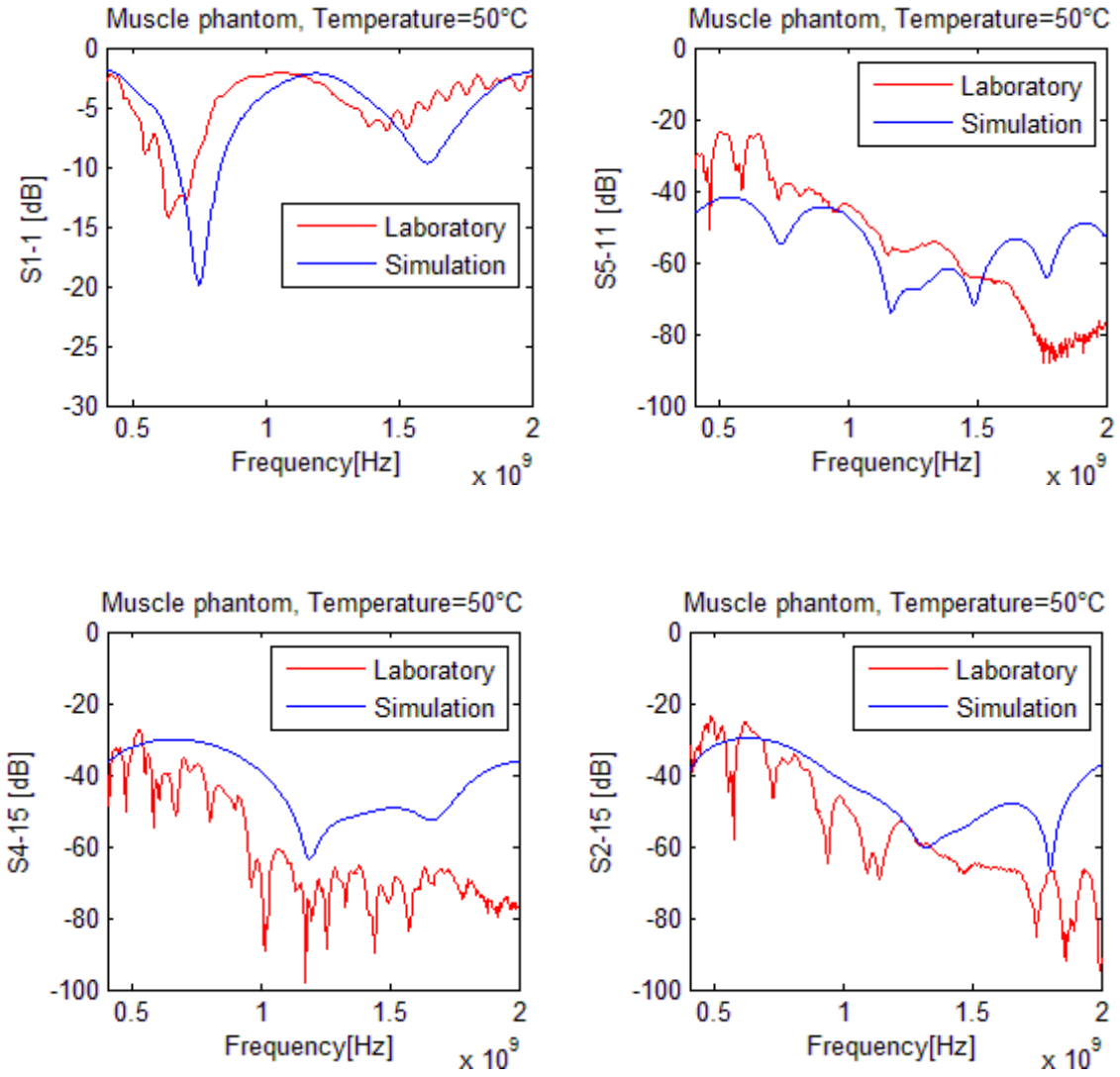

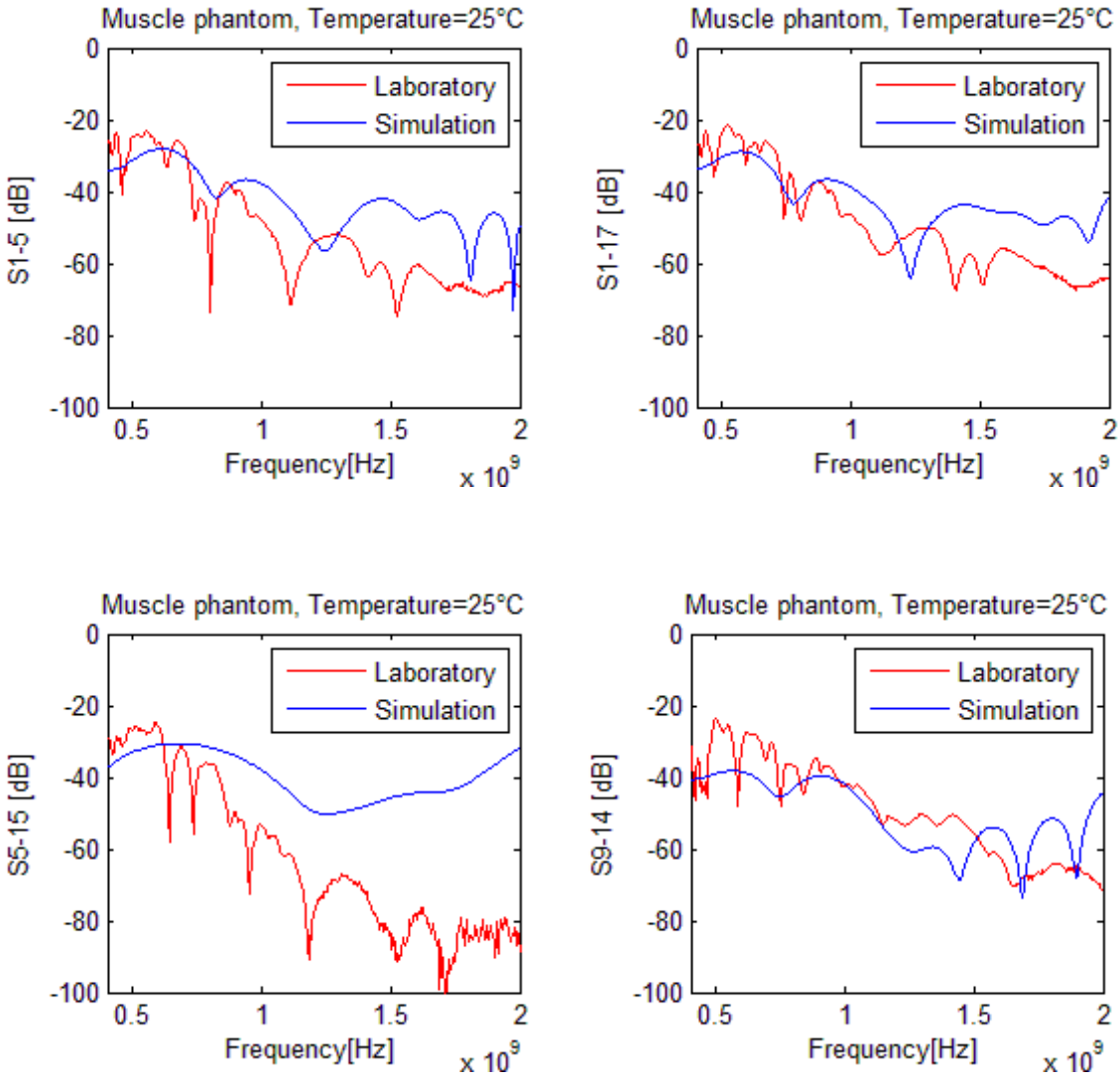

Figure A.5: Different phantom plots show the compatibility between measurement and simulation results. The temperature in the title represents the tumor object temperature with 20mm diameter located close to antenna 1.